8-2015

On The Spin Evolution Of Isolated Pulsars

Oliver Quinn Hamil
University of Tennessee - Knoxville, ohamil@vols.utk.edu

To the Graduate Council:

I am submitting herewith a dissertation written by Oliver Quinn Hamil entitled "On The Spin Evolution Of Isolated Pulsars." I have examined the final electronic copy of this dissertation for form and content and recommend that it be accepted in partial fulfillment of the requirements for the degree of Doctor of Philosophy, with a major in Physics.

William R. Hix, Major Professor

We have read this dissertation and recommend its acceptance:

Jirina R. Stone, Michael W. Guidry, Andrew W. Steiner, Joshua P. Emery

Accepted for the Council:

Carolyn R. Hodges

Vice Provost and Dean of the Graduate School

(Original signatures are on file with official student records.)

On The Spin Evolution Of Isolated Pulsars

A Dissertation Presented for the

Doctor of Philosophy

Degree

The University of Tennessee, Knoxville

Oliver Quinn Hamil

August 2015

For Melissa, without whom this endeavor would not have been possible.

Acknowledgements

I would like to thank, first and foremost, my advisor Jirina R. Stone for all of the guidance, discussion, postulation, invaluable criticism, and patience that helped bring this work to fruition. I feel lucky to have participated in research at a high level, and Jirina provided me with that opportunity. I am also very grateful for Nick J. Stone for insightful discussions and critiques, and for his advice concerning the physics in this thesis. I owe a debt of gratitude to our collaborators Martin Urbanec and Gabriela Urbancova for their contribution to our first paper, and for the hospitality they showed during our visit. Fridolin Weber and Rodrigo Negrieros have provided an incredible amount of support through discussions and the use of their respective neutron star codes, and have both tirelessly supported me over the years whenever I counted on their expertise regarding physics. They deserve my utmost appreciation. Lastly, I would like to thank those who have agreed to serve on my committee. I am grateful for your time and effort in the critique of this thesis and its content. A heart felt thanks to all.

Abstract

Neutron stars are the remnants of supernova explosions, and harbor the densest matter found in the universe. Because of their extreme physical characteristics, neutron stars make superb laboratories from which to study the nature of matter under conditions of extreme density that are not reproducible on Earth. The understanding of QCD matter is of fundamental importance to modern physics, and neutron stars provide a means of probing into the cold, dense region of the QCD phase diagram.

Isolated pulsars are rotating neutron stars that emit beams of electromagnetic radiation into space which appear like lighthouses to observers on Earth. Observations of these objects have been documented with very high accuracy. Measurements of pulsar rotational velocity, along with its first and second time derivatives, show that they slow down over time. The generally accepted explanation for the spin-down is that the pulsars behave like giant magnetic dipoles that lose energy in the form of electromagnetic radiation. This assumption of magnetic dipole radiation (MDR) leads to a general power law constructed from observation and governed by the braking index n, which relates the frequency to spin-down. The theoretical value for n is exactly 3 for MDR, but accurate observational measurements consistently yield values between 1.0 and 2.8.

The goal of this thesis is to improve understanding of the braking index through a two pronged investigation into this important quantity. We develop a frequency dependent model of the braking index that allows changing moment of inertia of the

star, and changes in magnetic field properties in the MDR torque mechanism. For the first time, we use physically realistic equations of state, along with state of the art computational codes to determine the dynamic neutron star properties required. We probe the stars at constant baryonic rest masses ranging from 1.0 to 2.2 solar masses over a range of frequency spanning from zero to the Kepler frequency for each star. We also develop a toy model of two interacting dipoles to make a first attempt at describing a plausible scenario by which the pulsar magnetic moment may evolve in time.

Table of Contents

List of Tables

List of Figures

Chapter 1

Introduction

Neutron stars are the remnants of supernova explosions, and are among the most dense objects in the universe. They have typical radii of about 10 km, masses between 1 and 2 times the mass of the sun ($M_\odot$), and can spin at a rate of hundreds of rotations per second (Weber, 1999; Glenndenning, 2000; Arnett and Bowers, 1977; Baym, 1978; Glendenning, 1985). Neutron stars harbor the densest stable matter that exists in the universe (Weber, 1999; Ozel et al., 2010; Lattimer and Prakash, 2004). The density at the cores of neutron stars can be as much as 5 – 10 times the density of atomic nuclei (ε_0). At such high densities, ordinary protons and neutrons are compressed so tightly that new particles and novel states of matter may be formed, such as hyperons ($\Lambda, \Sigma^{+,0,-}, \Xi^{0,-}$), boson condensates ($\pi^-, K^-$), superfluid and superconductive matter, and even deconfined quark matter. It has been hypothesized that some neutron stars may be composed entirely of absolutely stable quark matter, which could be more stable than the most stable atomic nucleus, ^{56}Fe (Glenndenning, 2000; Weber, 1999). The possible composition of compact stars (neutron stars, quark stars, or hybrids) is shown in Figure 1.1. Modeling these objects is difficult because the composition at the core is almost completely unknown, and so the interactions must be modeled for 10^{57} particles based on a few known low density parameters, creating both theoretical and computational challenges. The nature of ultra-dense matter is an open question

with important implications for nuclear and particle physics, as well as astrophysics. One important goal of neutron star research is to cohesively bridge the gap between the theory describing these objects, and the increasing amount of highly accurate observational data being collected.

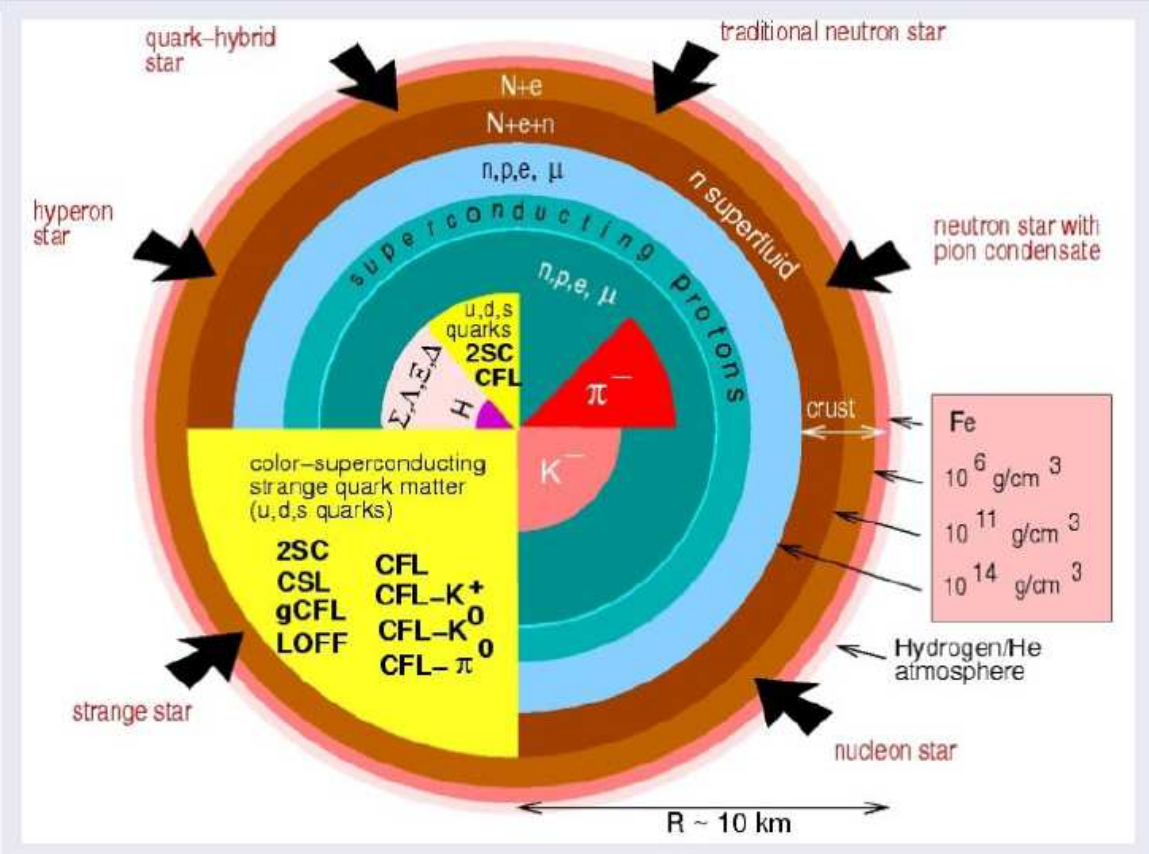

Figure 1.1: Cross sectional view of the possible composition of neutron stars based on different models of ultra-dense matter. Image Credit: Weber (2013)

At the forefront of modern physics is the study of matter at extreme temperature and density. The behavior of matter at extremely high temperatures and/or densities is of key importance to understanding the theory that governs hadronic matter; quantum-chromo-dynamics (QCD). Experiments at heavy-ion colliders such as RHIC and LHC probe the hot quark-gluon-plasma (QGP), which is the state of hadronic matter thought to exist in the very early universe. The phase-diagram of ultra-dense baryonic matter is shown in Figure 1.2. The phase diagram is a qualitative

description of the behavior of hadronic matter on a scale of density and temperature. The lower left corner of Figure 1.2 represents ordinary nuclear matter (i.e. protons, and neutrons), and one important goal of modern physics is to probe the regions of the diagram for increasing temperature and density. Experiments proposed for the Facility for Antiproton and Ion Research (FAIR) (GSI, 2012) hope to probe into the high density, high temperature region of the QCD phase diagram as a complement to investigation of the high temperature, low density region at LHC, and RHIC. Because of the attributes described above, neutron stars provide excellent laboratories for the study of cold, high density hadronic matter into the lower right region of the QCD phase diagram. Neutron star research complements Earth-based probes such as RHIC, LHC, and FAIR, in understanding the nature of dense hadronic matter.

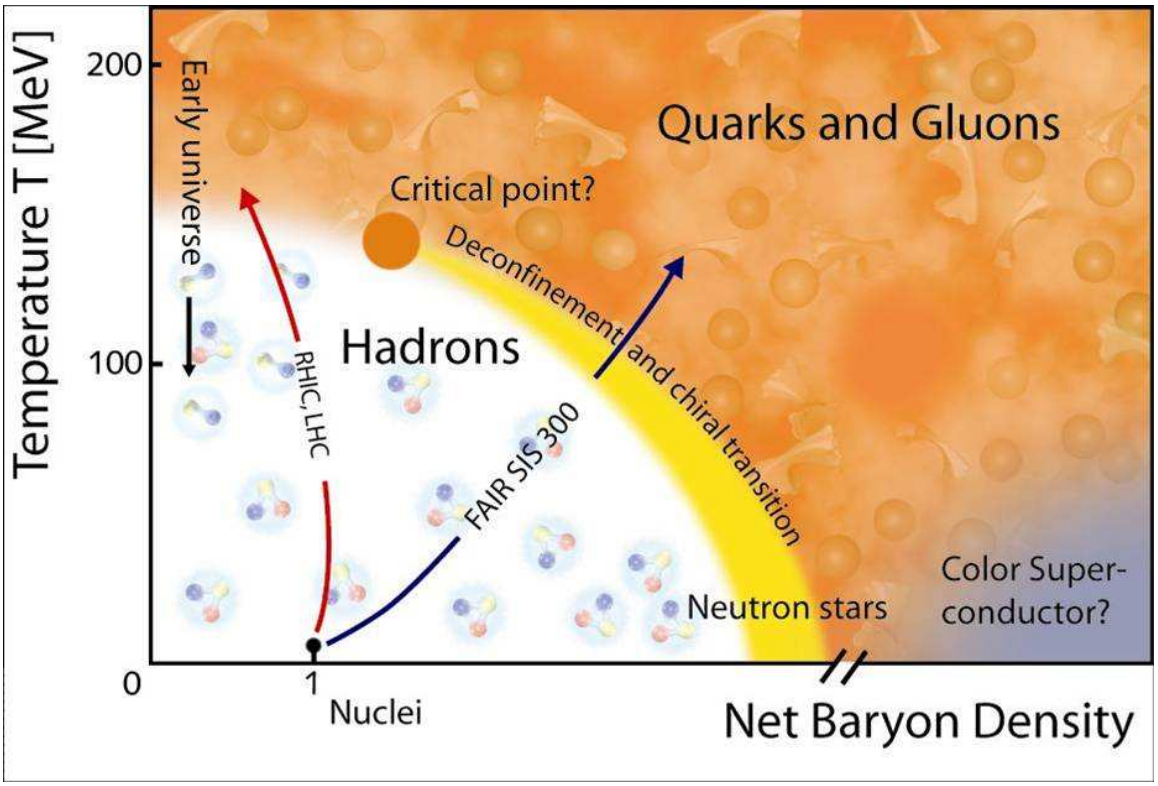

Figure 1.2: Phase diagram of baryonic matter. The early universe is represented by the low density/high temperature regime. Ordinary matter (protons / neutrons) exists at low temperatures and low densities, and neutron star matter is at the high density and low temperature regime. Image Credit: FAIR website GSI (2012).

Advancements in observations have led to an increase in high-quality neutron star data. Missions like the ROSAT MPI (2012) and XMM-Newton ESA (2012) have collected an unprecedented amount of observational data which allows for the testing of competing neutron star models. Numerical neutron star models are paramount in the understanding and interpretation of such data, and the accurate prediction of observable properties from microscopic models is key to understanding the ultra-dense QCD matter existing at the neutron star core.

While current understanding of neutron star composition, specifically in the core, is not well known, there exist constraints on the physics and particle interactions which lead to some reasonable models. Based on known nuclear properties in ordinary matter, extrapolation into high densities is possible. The microphysics governing neutron star composition is manifested in the equation of state (EoS). The correct description of known bulk properties, along with reasonable assumptions of energy-density and pressure within the star can predict the particle composition with some amount of accuracy. Figure 1.1 gives an illustration of some possible configurations of matter contained in the neutron star. Reliable observations of neutron star properties can constrain the possible particle composition. For example, high quality mass-radius observations can help to determine the central density which greatly affects the nature of the EoS, and the microphysics by extension.

There are direct and indirect observable properties of neutron stars which can be related to physical theory. Astronomers can measure mass (in binary systems), frequency (in pulsars), and energy loss by observing luminosities in pulsars and nebulae surrounding the supernova remnants. Other physical quantities described in neutron stars must be modeled based on these few observables. Pulsar frequency measurements can be highly accurate, and can be used to constrain model predictions of many neutron star properties ranging from energy-density profiles, to cooling processes and the age of the pulsars themselves.

One important quantity related to pulsar frequency is the so-called braking index, n. The braking index is a unitless quantity derived in the framework of total

(measurable) energy loss as it relates to the rotational energy of a pulsar, and is directly calculated from the observed frequency, along with the first and second time derivatives thereof. The accuracy of these observations allows for highly reliable braking indices to be calculated from observed frequencies. Because of the reliability of this data, the braking index serves as a good test for theory. Unfortunately, given the framework of the current theory, the most reliably measured data does not agree with the predicted values from theory.

The current, most readily accepted model for braking index is derived in the framework of magnetic dipole radiation (MDR). This model directly relates the loss of rotational energy to that of a large magnetic dipole rotating in space. The magnetic moment of the dipole is assumed to be misaligned to the axis of rotation which radiates electromagnetic energy as it spins. This assumption is an obvious first step in identifying the spin-down mechanism in pulsars simply because we can measure the radiated energy. There are some competing theories for the braking index mechanism, but it is widely accepted that the MDR model is dominant because the radiated energy is seen (i.e. pulsars), and can account for the large magnetic field assumed to exist in supernova remnants.

The goal of this research is to improve understanding of the braking index mechanism, and to make attempts to bring prediction from theory closer to reliable observed values. Our approach will be a two pronged investigation into the currently accepted MDR model. The challenge will be to explore a fully dynamical derivation of the braking index model based on state of the art calculations of the neutron star macro-properties pertinent to the spin-down torque mechanism in the model.

We can improve the model within this framework by applying frequency dependent, dynamic quantities such as moment of inertia (MoI) and magnetic field, calculated from physically realistic EoS, to the braking index model. These changes, along with the introduction of a simulated superfluid effect are used to converge theoretical braking index predictions with observed values as a function of frequency. The investigation requires two perspectives which will be outlined below. At high

frequencies, the braking index is dominated by MoI, and is susceptible to change across different microphysical descriptions. At frequencies below about 150 Hz, the braking index is dominated by the dynamics of the governing torque mechanism in the MDR model. The full investigation from these perspectives will provide a clearer understanding of the MDR braking law, and the relevant need for competing mechanisms can be better established.

Lastly, the braking index model derived can be used as a control for new considerations. Any new developments beyond the MDR model can be tested in the framework of dynamical changes occurring in the macroscopic properties of neutron stars. In particular, the magnetic field considerations are applicable to all proposed braking index models, and MoI is important to the density profile and composition of neutron star matter. We aim to provide a benchmark which moves our understanding of the braking index forward.

1.1 Neutron Stars Background Motivation

Isolated pulsars are assumed to be rotating neutron stars. Some of these objects, shown in Table 1.1, have a highly accurately measured angular velocity Ω, and corresponding time derivatives which show unambiguously that they are slowing down. One quantitative measure of the spin-down rate of a rotating pulsar with a constant moment of inertia (MoI) is the so-called braking index n (for definition see Section 1.2) which relates the rate of change in the angular velocity Ω to the n^{th} power of Ω. Goldwire and Michel investigated this result in their quadratic least-squares analysis of the time dependence of the period of Crab pulsar using data available in 1967 and found $n = 5 \pm 3$ (Goldwire and Michel, 1969). Current highly refined observations and analysis yield much more precise data on the rotational period of pulsars, and the first and second derivatives of the rotational frequency ($n = 2.51 \pm 0.01$ for the Crab pulsar). The third derivative is known for the Crab pulsar (Lyne et al., 1988), and PSR B1509-58 (Kaspi et al., 1994). Extraction of this data

Table 1.1: Selected pulsars adopted from Magalhaes et al. (2012); Espinoza et al. (2011); Lyne et al. (2015). $n_{\rm freq}$ is the value of n obtained for the given pulsar, at the given frequency, with changing MoI calculated in this work.

PSR	Frequency (Hz)	n	$n_{\rm freq}$	Ref.
B1509−58	6.633598804	2.839±0.001	2.999	Livingstone et al. (2007)
J1119−6127	2.4512027814	2.684±0.002	2.999	Waltevrede et al. (2011)
J1846−0258	3.062118502	2.65±0.1	2.999	Livingstone et al. (2007)
		2.16±0.13		Livingstone et al. (2011)
B0531+21	30.22543701	2.51±0.01	2.995	Lyne et al. (1993)
B0540−69	19.8344965	2.140±0.009	2.997	Livingstone et al. (2007)
				Boyd et al. (1995)
J1833−1034	16.15935711	1.8569±0.001	2.999	Roy et al. (2012)
B0833−45	11.2	1.4±0.2	2.999	G. et al. (1996)
J1734−3333	0.855182765	0.9±0.2	3.000	Espinoza et al. (2011)

from observation involves a detailed analysis of the time evolution of the pulses, and of the spectra and luminosity of radiation from the related nebulae in a wide range of wavelengths. Although data on many pulsars are available in the literature, there are only eight pulsars generally accepted to yield reliable values of the braking index as displayed in Table 1.1.

Observation of the periodic emission of large amounts of electromagnetic radiation from pulsars has led to a plethora of models attempting to explain this phenomenon. Following the work of Pacini (1967, 1968), the first association between pulsars and neutron stars was made by Gold (1968, 1969), who showed that a rotating neutron star with surface magnetic fields of $\sim 10^{12}$ gauss could account for many properties of pulsars, including the pulse polarization, and the increase in period. The loss of rotational energy was identified with the emission of electromagnetic waves (radio emission), exerting a radiation reaction as a drag on the spin of the star. Another model for energy loss was introduced by Michel (1969), who considered acceleration of charged particles, and massive winds. Ostriker and Gunn (see Ostriker and Gunn (1969), and refs. therein) qualitatively explored a model for energy loss through multipole radiation. They showed that a pulsar can emit a large amount

of low frequency magnetic dipole and gravitational quadrupole radiation, which is very efficient in accelerating charged particles to relativistic energies. The energy losses due to the radiation were associated with losses of angular momentum, and increase in the rotational period of the star. Considering the star to be a magnetized sphere rotating in vacuum, with a magnetic moment misaligned at a fixed angle to its axis of rotation, the surface magnetic field strength was estimated using the measured change in angular velocity. Although the existence of the highly conducting, co-rotating magnetosphere, and the interstellar medium (plasma), consisting of relativistic particles accelerated up to the speed of light may theoretically affect the calculation, it was neglected, but the order of magnitude of the calculated field strength by Goldreich and Julian (1969) did not differ considerably from a more rigorous estimate currently in use (Reisenegger, 2003).

The value of n provided by observations is deduced without any preconceptions about the physical nature of the pulsar. Goldwire and Michel (1969) performed a least-squares analysis of the time dependence of the period of the Crab pulsar, and showed that $\dot{\Omega} = -K\Omega^n$, is an acceptable fit to the data. The value of n is dependent on the mechanism used to describe the origin of the energy loss of the rotating pulsar. Theoretical models based on different scenarios for the origin of the energy loss by the pulsar yield different values of n. In the idealized case, when the magnetic field is modeled as a pure dipole, MoI, and surface magnetic field strength are constant, and the star rotates in vacuum, the value of the braking index is always $n = 3$. It is widely assumed that most pulsars spin-down due to magnetic dipole radiation (MDR) because it is the best model for the origination of the pulse itself. The MDR, as stated above, is assumed to provide a reliable enough estimate for the magnetic field strength of pulsars, so that it is the basis for the calculation of the magnetic fields of all pulsars that cannot be measured directly (as in some magnetars). Despite being inconsistent with measured braking index values, the MDR model likely accounts for some portion of spin-down for all pulsars. Consideration of radiation produced by a relativistic outflow of a pulsar wind

from the surface of the rotating star leads to $n = 1$ (Michel, 1969; Harding et al., 1999) (although n = 2 was also considered by Carraminana and Alvarez (1996)), and emission of gravitational quadrupole radiation requires $n = 5$ (Ostriker and Gunn, 1969). Several authors note that the emission of gravitational radiation is unlikely to compete with the other mechanisms at present because observations of braking index n are consistently less than three. However, it cannot be ruled out that it plays an important role at earlier times in the lifespan of pulsars. The relation between emission of gravitational waves, and braking index of young pulsars was studied in detail by Alford and Schwenzer (2014). A combination of these mechanisms was considered by Alvarez and Carraminana (see Carraminana and Alvarez (2004) and refs. therein) in their multipole spin-down equation. Most recently, Liu et al. (2014), studied particle wind energy loss in intermittent pulsars and its role in the rate of spin-down.

There is extensive literature about observational data for the rotational period of pulsars, and the first, second, and third time derivatives thereof for the Crab pulsar (Lyne et al., 1988), and PSR B1509-58 (Kaspi et al., 1994). The extraction of this data from observation involves a detailed analysis of the time evolution of the pulses, and of the spectra and luminosity of radiation from the related nebulae in a wide range of wavelengths. There are currently only eight pulsars which are generally accepted to have reliably measured values of their braking indices. We summarize data on these pulsars in Table 1.1. Examination of the tabulated values shows immediately that the simple model of a pulsar as a rotating magnetic dipole field in vacuum, yielding $n = 3$, does not agree with the results of precise observations. Most models track the time evolution of the pulsar spin-down through the $P - \dot{P}$ diagram (e.g., Carraminana and Alvarez (2004); Contopoulos and Spitkovsky (2006)). Introduction of time dependence of constants in the power law may lead to closer agreement between models, and observation; however, it can only introduce a speculative time dependence of observables, usually of the magnetic field (see e.g. Blanford and Romani (1988); Contopoulos and Spitkovsky (2006); Zhang and Xiee (2012);

Gourgouliatos and Cumming (2014)). Alternatively, modifications of the co-rotating magnetosphere have been considered (Melatos, 1997). As our observations span, at best, 50 years, they offer only a short snapshot of the time history of a pulsar, and definitive information regarding long-term time dependence of the slow-down mechanism, and variations from pulsar to pulsar is still not available.

As we have seen, Table 1.1 shows that the ideal model of a pulsar as a magnetic dipole rotating in vacuum does not agree with the results of precise observations. There have been many attempts to extend/modify the basics of the model. These include consideration of magnetic field activity, superfluidity and superconductivity of the matter within pulsars, and modifications of the power law and related quantities. However, there is not a model currently available which would yield, consistently, the typical spread of values of n as illustrated in Table 1.1. It is not the objective of this thesis to give a comprehensive survey of all attempts to achieve consistency between theory and observation. We only mention examples of some recent work, mainly related to the pulsars with reliable braking indices.

Livingstone et al. (2011) surveyed several promising models of the relation between magnetic activity and the neutron star spin-down, including an increasing magnetic moment, (e.g. Blanford and Romani (1988); Lyne (2004)), and the effects of magnetospheric plasma on the spin-down torque, (e.g. Harding et al. (1999); Kramer et al. (2006)). There has been an interesting observation of a permanent change of the braking index of PSR J1846-0258, which exhibited distinctly magnetar-like behavior in May-July, 2006. With an initial braking index of 2.65±0.01, this pulsar exhibited a strong magnetar-like outburst, and a post-burst measurement yielded a braking index of $n = 2.16 \pm 0.13$ (Livingstone et al., 2011). No fully successful explanation of this phenomenon has been found as of yet, but variability in magnetospheric plasma remains a promising direction for future consideration, especially in light of the recent report of variable spin-down rate correlated with radio pulse shape changes for several pulsars, confirming a link between torque, and emission properties in several pulsars (Lyne et al., 2010).

Another interesting object, PSR J1734-3333, with a very low braking index, $n = 0.9$, has attracted a lot of attention. Espinoza et al. (2011) suggested that PSR J1734-3333 may be a potential magnetar, whose magnetic field has been buried under the surface due to large accretion shortly after the supernova explosion, and is relaxing out of the surface at present. The increasing of magnetic field strength may also result in the small braking index value of 0.9. Very recently, Liu et al. (2014) proposed another interpretation for the small braking index as a consequence of a fall-back disk around PSR J1734-3333 that is braking the pulsar by accreting matter with opposing angular momentum.

It is supposed that superfluidity and superconductivity may exist in the inner crust and cores of neutron stars. The effects of superfluidity on the angular momentum of a pulsar, and thus on the changes of its rotational period have beed studied mostly in connection with glitches, observed primarily in young, fast rotating pulsars. In determination of the braking index, glitches are normally ignored because they happen on very short timescales relative to the overall spin-down of the pulsar, and thus do not effect the spin evolution over the life of the star. Ho and Andersson (2012) provide a model based on a decrease in the effective MoI due to an increase in the fraction of the stellar core that becomes superfluid as the star cools through neutrino emission. The main assumption in their model is that core superfluid neutrons are allowed to decouple and pin. However, it is not clear whether this mechanism can be strong enough to act in the way assumed in Ho and Andersson (2012). Page et al. (2014) extensively reviewed stellar superfluids, including a possible connection between the occurrence of superfluidity in rotating pulsars and their spin-down rates, but no solution to the braking index issue was suggested.

Modifications of the canonical MDR models have also been attempted by many authors. For example, Johnston and Galloway (1999) used the standard equation for the spin-down of a neutron star, and derived a formula for the braking index via integration rather than the conventional differentiation. The new formula has the advantage that it depends only on the first derivative of the rotational frequency.

However, this formula was applied to cases apparently affected by glitches and, although it reproduced the braking index of the Crab pulsar, its success was not realized for other cases where glitches can be eliminated from the data. Recently, Magalhaes et al. (2012) reported results of a study concerning determination of the braking index based on a modification of the MDR model, which admits that pulsars are rotating magnetic dipoles, but allows for a variable braking index in the braking torque equation. Their statistical approach produced a satisfactory agreement with observation, but only due to introduction of an empirical parameter which varies from pulsar to pulsar, and is not motivated by any known physical considerations, i.e. it is purely a numerical fit.

The evolution of the angle of inclination between the rotational axis of the star and the dipole has been considered with interesting results. Lyne et al. (2013) have investigated the effects of an increasing inclination angle on braking index. The commons assumption so far has been that, over time, the magnetic moment should align itself with the axis of rotation, but there is new observational evidence that the dipole is, in fact, migrating toward the equator of the star. The time rate of change of the angle of inclination α may affect the braking index, especially at low frequencies where changes in the MoI are negligible, and the magnetic field strength is constant. Lyne et al. (2013) showed that the correct model of this change in angle can account for the current braking index of the Crab pulsar. Their results indicate that the change in α with the correctly associated current value for α can reproduce the measured braking index in the Crab pulsar. These results are very interesting in that they achieve a solution for the very slowly rotating pulsars where changes in MoI are insignificant. This idea is discussed further in Section 1.2.

In this thesis, we focus first on finding the full dynamical range of the MDR model yielding a maximum physically meaningful deviation from the canonical value of the braking index, $n = 3$, as a function of rotational velocity. The effects of variation in the MoI of a rotating pulsar have been, in the spirit of analysis by Glendenning (2000), fully derived and included in the calculation, using two independent computer

codes, and four physically realistic Equations of State (EoS). We have also simulated an effect of superfluid conditions at the threshold between the crust and core energy density, inside the star, which eliminates the core contribution of angular momentum to the calculation. For the low frequency region of the braking index curve, MoI and surface magnetic field strength in the MDR model are essentially constant, which leads to the canonical $n = 3$ for any object rotating at less than about 150 Hz. In order to account for observed braking indices less than $n = 3$ in this 'low-frequency' range, we look at the inclination angle of the magnetic moment to the axis of rotation, and attempt to produce a function which varies in a way that reduces the braking index values similar to the research by Lyne *et al.* discussed above.

1.2 Braking Index: Open Questions

It is important at this point to identify the main braking index mechanism, why it is important, and how we can expect a frequency dependent model to behave. We find that there are two ends to the dynamics of the braking index that are dominated by different mechanisms in the braking law (Hamil, 2014). In this section we will motivate the dynamical treatment of the braking index and set up the main problems to be addressed in this thesis.

As stated earlier, isolated pulsars are assumed to be rotating neutron stars with accurately measured angular velocities Ω, that tend to slow down over time. Processes, including the emission of gravitational radiation, and of relativistic particles (pulsar wind), are considered along side the most common MDR model as explanation to the observed spin-down. The calculated energy loss by a rotating pulsar is assumed proportional to a model dependent power of the rotational velocity, Ω. This relation leads to the power law $\dot{\Omega} =$ -K Ω^{n} where n is called the braking index. Precise calculation of the braking index has been achieved for a small set of very accurately measured pulsars, and the results are in the range $1 < n < 2.8$. The

correct model of the physics of pulsar spin-down should match the observed values. No such model exists to date.

1.2.1 Definition

The pulsar spin-down rate is an observation that has been recorded for the past few decades. That pulsars can be seen and measured is evidence of the electromagnetic radiation emanating from what is assumed to be a strong dipole misaligned with the axis of rotation. This misaligned dipole is generally considered to dominate the pulsar spin-down as it accounts for rotational energy being carried away from the star (Pacini, 1967, 1968; Gold, 1968, 1969; Goldwire and Michel, 1969). The observed loss of energy is modeled, as shown above by $\dot{\Omega} =$ -K Ω^{n} where n is the braking index. The braking index itself is a purely observational parameter which is determined from pulsar timing observations along with their first and second derivatives (see, e.g., Lyne et al. (2015))

$$n = \frac{\Omega\ddot{\Omega}}{\dot{\Omega}^2}. \tag{1.1}$$

The value for the braking index n is theoretically determined by the torque mechanism working counter to the rotation of the star. In the simple MDR model, the radiating dipole carries energy away from rotation thereby producing a torque which slows the rate of rotation of the pulsar. This is the main assumption for pulsars because of the nature of the observed radiation, but there are at least two other acceptable possibilities for the torque mechanism. The emission of charged particles, accelerated to relativistic velocities, forming a massive wind from the surface of the pulsar (Michel, 1969; Harding et al., 1999) may play a role in spin-down. Another consideration is higher order multipole electromagnetic radiation, or gravitational quadropole components to the radiated energy (Ostriker and Gunn, 1969; Alford and Schwenzer, 2014). For each mechanism described above, the theoretical braking index is $n = 1, 3, 5$ for particle wind, MDR, and quadrupole radiation, respectively.

1.2.2 MDR Issue

Of the mechanisms described above, the most readily accepted is the MDR model. This model predicts the radiated energy expected from a magnetized sphere rotating in vacuum (the accepted description of pulsars). The braking index value for the MDR model is $n = 3$. We see in Table 1.1 eight pulsars with accurately observed spin evolution. The given values for the braking index are accurate to within a few percent or better. It is clear that none of these observed stars has a braking index consistent with any of the values produced from theory.

There is a clear deviation between observed braking index values, and those calculated from theory. The static value associated with each torque mechanism (MDR, wind, quadrupole) is directly due to the treatment of the differential equation governing braking index. Each mechanism has the differential form,

$$\dot{E} = -C\Omega^{n+1}, \tag{1.2}$$

where C contains the physics of the associated mechanism, Ω is the rotational velocity, and n is the braking index. Likewise, the rotational energy of a rotating sphere is given by,

$$\dot{E} = \frac{d}{dt}(\frac{1}{2}I\Omega^2), \tag{1.3}$$

where I is the moment of inertia. Setting the above two equations equal to each other leads to the braking index power law. There are two different ways to consider the evolution of the power law. Firstly, we can assume the moment of inertia is constant in time which leads to the known power law,

$$\dot{\Omega} = -K\Omega^n, \tag{1.4}$$

where $K = C/I$. If K is a constant (static case), this leads to the given values described earlier of $n = 1, 3, 5$. However, if we consider that the moment of inertia changes over time, and that the physical values contained in the mechanism (C) may change with time (or frequency), this leads to the braking index as a function of Ω,

$$n(\Omega) = n_0 - \frac{3\Omega I' + \Omega^2 I''}{2I + \Omega I'} + \frac{C'\Omega}{C}, \tag{1.5}$$

where n_0 is the theoretical (static case) braking index associated with each torque mechanism, and the prime notation denotes derivatives with respect to angular frequency. It will soon be evident that there are two ways in which the evolution of the braking index may proceed. From Eq. 1.5, the change in MoI is clear, but what is less clear is the meaning of C and C'. The physics of each torque mechanism is contained in C, and C' gives the change with respect to frequency of the values describing the physics. For example, in the MDR model, C contains the magnetic moment, which may change with frequency.

As we see from the above equations, the simple values for braking index come from assumptions that the moment of inertia of the star is constant (or that the star is static), and the parameters defining the physics of the braking torque are all constant. This means that composition, magnetic field, rotational effects, etc., have no effect on braking. The frequency dependent solution (Eq. 1.5) allows for the problem to be explored in much greater detail. The microscopic properties of the star must be considered in order to have a cohesive model which allows for changing values which may affect the braking index.

1.2.3 Moving Forward

The frequency dependent solution to the braking index allows for the problem to be approached from two extreme positions. There can be a dependence on frequency where the moment of inertia changes at a rate which brings the braking index away from the canonical value, or, in the limit of very slow rotation, the parameters

governing the torque mechanism can be changing with frequency (or time). Close examination of Eq. 1.5 shows that changing moment of inertia can have a significant effect on the braking index at high frequencies, but in the limit that moment of inertia changes very slowly with frequency, there is still a term allowing for the physics in the torque mechanism (C) to change. In the assumed MDR model, high frequency calculations show a reduction in braking index consistent with observation; however, the observed pulsars in Table 1.1 are all rotating at low frequency. It will be shown in Sections 2.1 that the effect of changing moment of inertia over a range of frequency up to 160 Hz, assuming constant C, is negligible. It is clear that below this frequency, there is no change in moment of inertia, and the subsequent MoI dependent deviation from $n = 3$ is also insignificant. Noting that the data in Table 1.1 spans a range of frequencies between about 1 - 30 Hz, it is worthwhile to consider changes in the physical parameters of the torque mechanisms at low frequency.

1.2.4 Mechanism

It is important to model pulsar braking indices for frequencies consistent with the accepted observations. This can be approached in a few different ways. The first thing to examine is the dependence on C in Eq. 1.5. For example, in the MDR model we have,

$$C \propto \mu^2 \sin \alpha^2, \tag{1.6}$$

where μ is the magnetic moment and $\sin \alpha$ is the angle of inclination between the magnetic moment and the axis of rotation. It is clear from Eq. 1.5 that one or both of these values would have to increase as the pulsar spins down to move toward the observed braking index values that are less than $n = 3$. It has been suggested that there is some observational evidence that $\sin \alpha$ is increasing with time (Lyne et al., 2015).

Effects on the magnetic field may be a factor for all three accepted torque mechanisms. The magnetic field may increase, decrease, or change alignment (Contopoulos and Spitkovsky, 2006). The torque may vary with magnetic field in a way that is not a pure dipole. Plasma outflow may cause currents in the magnetosphere. Interaction with the magnetosphere in general may play in the torque mechanism (Livingstone et al., 2011). Rotationally-driven effects such as first order phase transitions in the core neutron star matter, changes in the density profile, and superfluidity may also affect the magnetic field. The evolution of the magnetic field is most readily applied to the MDR model, but it is also important for the relativistic wind, and higher order magnetic field terms.

Particles near the surface of the star can be accelerated to relativistic energies, and thus carry away rotational energy from the pulsar in the form of a particle wind. The wind mechanism also has a dependence on the magnetic field, and thus all of the considerations explained above can affect the braking index due to the wind. The braking index value for the wind is $n = 1$, which is near the lowest measured braking indices shown in Table 1.1. Since all values fall between 1, and 3, it is prudent to consider the wind as a possible torque mechanism affecting braking.

1.2.5 Polynomial

The considerations outlined above require knowledge of the origin and distribution of the magnetic field which is not readily available. Also the nature of rotationally-driven effects is not well known. This poses a problem in that there is some speculation involved in trying to relate braking index values to changes in the magnetic field or other similar physics in the torque mechanisms which leads to a phenomenology that is not necessarily physical.

Another approach to this problem considered by Carraminana and Alvarez (2004) is to expand the braking law itself into a polynomial which consists of all assumed torque mechanisms. In this way, the low frequency variation in the braking index

can be explored while we can assume there are no changes in the magnetic field, composition of the star, magnetosphere, etc. Given that the accurately measured braking indices range in value from about $1 - 2.8$, it is prudent to explore a solution in which the braking index results from a combination different of torque mechanisms.

As shown in (Carraminana and Alvarez, 2004), the braking law can be expanded as,

$$\dot{\Omega} \quad = \quad -s(t)\Omega - r(t)\Omega^3 - g(t)\Omega^5, \tag{1.7}$$

where $s(t)$, $r(t)$, and $g(t)$ are functions representing the wind, MDR, and quadrupole torque mechanisms respectively, and Ω is the rotational frequency.

The polynomial can be used to fit the known braking index values. The braking index range of roughly $1 - 3$ indicates that the combination of wind ($n = 1$) and MDR ($n = 3$) should be important. The quadrupole ($n = 5$) may not play a role at low frequencies. Furthermore, the combination of $s(t)$ and $r(t)$ may constrain the magnetic field. The polynomial solution may also be expanded into high frequencies which may constrain other rotationally dependent effect on mass, composition, and magnetic field.

This polynomial approach is not considered in this thesis, but is relevant to the braking index issue, and should be explored in the future as complement to the present work. Magnetic field evolution, along with other dynamic effects are first cataloged, so that in the future they may be applied to the polynomial approach for a more cohesive investigation of all possible constraints on the low to high frequency braking index model.

1.2.6 Summary

The braking index problem can be approached from two ends. We can consider very fast rotation where moment of inertia may dominate the spin evolution, or we can consider very slow rotation where the physics of the braking mechanism must be

changing to describe the observed data. As will be shown later, the braking index is dominated by the torque mechanisms at frequencies below about 160 Hz. Above this frequency, changes in moment of inertia due to deformation of the star become increasingly important. Unknown composition and magnetic field dynamics play a crucial role in understanding the braking index, and are important to magnetic dipole radiation and relativistic wind at low frequency. These effects are difficult to model as they are not yet well understood.

The high and low frequency ranges can be probed in the theory by first allowing for changes in MoI to affect the braking index as a function of frequency in the limit that the deformation of the star occurs. Secondly, at the low frequency range, arbitrary changes in the physics, for example, magnetic field strength and inclination, are allowed in order to affect the braking index. The change in inclination angle α is a likely candidate for first approximations of these mechanism changes.

In order to model braking indices without knowledge of magnetic field evolution or rotationally driven changes in composition, it is possible to construct a polynomial which will fit the data using functions of the known braking index mechanisms at low frequency. This model can be extended to high frequencies, and to include considerations of the unknown values described above. This can also be extended to include physical equations of state, and mass dependence.

A single, cohesive investigation of all the above possibilities is necessary to our understanding of pulsar spin evolution. The resulting parameters may help to constrain the poorly known micro-physics at work in the cores of rotating neutron stars.

In this thesis, we will exhaustively investigate the MDR model using realistic microphysics across all frequencies. The findings will be used in future work to extend the physical relevance of the polynomial approach, and to constrain possible rotationally driven composition changes in pulsars at high frequency.

Chapter 2

High frequency dynamical MDR

We turn our attention first to the dynamical derivation of the MDR braking index, and investigate the range of values it yields over the full range of frequency from zero to the Kepler (mass shedding) frequency for a given star. In this section, the results will include only those resulting from an allowed frequency dependent moment of inertia, MoI, as shown in our Phys. Rev. D publication (Hamil et al., 2015).

We assume that isolated pulsars are rotating neutron stars that are seen to be slowing down over time. Although the several mechanisms of the spin-down discussed in Chapter 1 may contribute, the commonly accepted view is that emission of magnetic dipole radiation (MDR) from a rotating magnetized body dominates. The calculated energy loss by a rotating pulsar with a constant moment of inertia is assumed proportional to a model dependent power of Ω. This relation leads to the power law $\dot{\Omega}$ = -K Ω^{n} where n is the braking index. The MDR model predicts n exactly equal to 3.

In this chapter we aim to determine the deviation of the value of n from the canonical $n = 3$ for a star with a frequency dependent moment of inertia in the region of frequencies from zero (static spherical star) to the Kepler velocity (onset of mass shedding by a rotating deformed star), in the macroscopic MDR model. For the first time, we use physically realistic Equations of State (EoS) of the star to determine

its behavior and structure as a function of spin rate. In addition, we examine the effects of the baryonic mass M_B of the star, and possible core superfluidity, on the value of the braking index within the MDR model.

Four microscopic Equations of State are employed as input to two different computational codes which solve Einstein's equations numerically, either exactly or using the perturbative Hartle-Thorne method, to calculate the moment of inertia and other macroscopic properties of rotating neutron stars. The calculations are performed for fixed values of M_B (as masses of isolated pulsars are not known) ranging from $1.0 - 2.2 M_\odot$, and fixed magnetic dipole moment and inclination angle between the rotational and magnetic field axes. The results are used to solve for the value of the braking index as a function of frequency, and find the effect of the choice of the EoS, and baryonic mass M_B. The density profile of a star with a given M_B is calculated to determine the transition between the crust and core of the star, and used in estimation of one possible effect of superfluidity on the braking index.

Our results show conclusively that, within the model used in this work, any significant deviation of the braking index away from the value $n = 3$ occurs at frequencies higher than about five times the frequency of the fastest of the rotating isolated pulsars most accurately measured to date. The rate of change of n with frequency is related to the stiffness of the EoS and the M_B of the star as this controls the degree of departure from sphericity. Change in the moment of inertia in the MDR model alone, even with the more realistic features considered here, cannot explain the observational data on the braking index, and other mechanisms must be sought.

The chapter is organized as follows: The braking index, as calculated in the canonical MDR model, and its extensions introduced in this work, are presented Sections 2.2–2.2.1. Section 2.3 contains the computational method employed in this work, followed by Section 2.4 where the main results are reported. The main findings of this work, and discussion are summarized in Section 2.6.

2.1 The MDR braking index

The slowing down of rotating neutron stars has been observed and modeled for decades. The calculated energy loss by a rotating pulsar is assumed proportional to a model dependent power of Ω. This relation leads to the previously discussed power law $\dot{\Omega}$ = -K Ω^n where n is the braking index. The value of n can be, in principle, determined from observation of higher-order frequency derivatives related to n by Lyne et al. (2015)

$$n = \frac{\Omega\ddot{\Omega}}{\dot{\Omega}^2} \tag{2.1}$$

$$n(2n-1) = \frac{\Omega^2\dddot{\Omega}}{\dot{\Omega}^3}. \tag{2.2}$$

When the star is assumed to be a magnetized sphere, rotating in vacuum, with a constant moment of inertia (MoI) and a constant magnetic dipole moment, misaligned at a fixed angle to its axis of rotation, n is equal to 3 (for derivation see Section 2.2). Extraction of the rotational frequency and its time derivatives from observation involves a detailed analysis of the time evolution of the pulses, and of the spectra and luminosity of radiation from the related nebulae in a wide range of wavelengths. Although data on many pulsars are available in the literature, there are only eight pulsars generally accepted to yield reliable data - including rotational frequency and its first and second time derivatives - on the spin-down (see Table. 1.1, recent compilation Magalhaes et al. (2012) and Refs. therein). The third derivative is known only for the Crab pulsar Lyne et al. (1988), and PSR B1509-58 Kaspi et al. (1994).

As discussed in Chapter 1, examination of Table 1.1 shows that $n = 3$ does not agree with observation. There have been many attempts to extend/modify the basics of the MDR model. These include consideration of magnetic field activity (e.g., Livingstone et al. (2011); Blanford and Romani (1988); Melatos (1997); Lyne (2004); Harding et al. (1999); Kramer et al. (2006); Lyne et al. (2010)), superfluidity and superconductivity of the matter within pulsars (e.g., Sedrakian and Cordes (1998);

Ho and Andersson (2012); Page et al. (2014)), and modifications of the power law and related quantities (e.g., Johnston and Galloway (1999); Magalhaes et al. (2012)). Time dependence of the constants in the MDR model has also been considered (Blanford and Romani, 1988; Contopoulos and Spitkovsky, 2006; Zhang and Xiee, 2012; Gourgouliatos and Cumming, 2014). In particular, time evolution of the inclination angle between spin and magnetic dipole axes has been recently addressed (Lyne et al., 2015, 2013). However, there is no model currently available that would yield, consistently, the typical spread of values of n as illustrated in Table 1.1.

Models outside the MDR have also been introduced. For example, energy loss through emission of accelerated charged particles, forming a massive wind from the surface of rotating stars (Michel, 1969; Harding et al., 1999), or emission of higher multipole electromagnetic radiation, including the gravitational quadrupole component (Ostriker and Gunn, 1969; Alford and Schwenzer, 2014), has been studied. Competition of different mechanisms, MDR, emission of gravitational waves, and particle wind was also investigated by Carraminana and Alvarez (1996, 2004).

In this chapter we focus on determination of the maximum deviation of the braking index from the value $n = 3$ by introducing two modifications of the simple MDR model: frequency dependence of MoI, related to the change of shape of a deformable star due to rotation, and superfluidity at the crust/core interface of the pulsar. The correction to the expression of the braking index arising from these modifications is derived following Glendenning (2000), and included in the calculation, using four realistic Equations of State (EoS) over a range of baryonic mass (M_B). We study the relation between the stiffness of the EoS and the rate of change of the braking index as a function of frequency and the M_B. The four EoS were also used to obtain mass density profiles of the pulsars needed to determine the transition region between the crust and core. These results were utilized in the simulation of an effect of superfluid conditions that eliminates the angular momentum exchange at the radial threshold between the crust and core. The calculation is performed over a full range of frequencies of the pulsar from zero to the Kepler (mass shedding) frequency, and

a range of M_B from 1.0 to 2.2 $M_\odot$, representing a range of gravitational masses from about 0.8 to 2.0 $M_\odot$.

2.2 Simple MDR model

The total energy loss by a rotating magnetized sphere can be expressed in terms of the time derivative of the radiated energy as (Pacini, 1968; Glendenning, 2000; Lyne et al., 2015)

$$\frac{dE}{dt} = -\frac{2}{3}\mu^2\Omega^4\sin^2\alpha, \tag{2.3}$$

where μ is the magnetic dipole moment of the pulsar, $\mu = \mathrm{B\ R}^3$. R is the radial coordinate of a surface point with the surface magnetic field strength B, Ω is the rotational frequency, and α is the angle of inclination between the dipole moment and the axis of rotation (Glendenning, 2000).

Substituting the kinetic energy of a rotating body, dependent on the MoI I,

$$E = \frac{1}{2}I\Omega^2, \tag{2.4}$$

into (2.3) yields

$$\frac{d}{dt}\left(\frac{1}{2}I\Omega^2\right) = -\frac{2}{3}\mu^2\Omega^4\sin^2\alpha. \tag{2.5}$$

Assuming constant MoI, $dI/dt = 0$, we get

$$\dot{\Omega} = -\frac{2}{3}\frac{\mu^2}{I}\Omega^3\sin^2\alpha. \tag{2.6}$$

Setting $K = \frac{2}{3}\frac{\mu^2}{I}\sin^2\alpha$ in (2.6) and taking μ and α constant leads to the commonly used braking power law describing the pulsar spin-down due to dipole radiation:

$$\dot{\Omega} = -K\Omega^3. \tag{2.7}$$

Differentiating (2.7) with respect to time

$$\ddot{\Omega} = -3K\Omega^2\dot{\Omega}, \tag{2.8}$$

and combining (2.7) and (2.8) to eliminate K we get the value of the braking index n,

$$n = \frac{\Omega\ddot{\Omega}}{\dot{\Omega}^2} = 3. \tag{2.9}$$

2.2.1 MDR model with frequency dependent MoI

The simple MDR value $n = 3$ (Eq. 2.9) is derived taking I, μ, and α as independent of frequency and constant in time. However, in reality, the MoI of rotating pulsars changes with frequency and, consequently, with time (Glendenning et al., 1997; Glendenning, 2000). The equilibrium state of a rotating pulsar includes the effect of centrifugal forces, acting against gravity. The shape of the pulsar is ellipsoidal with decrease (increase) in radius along the equatorial (polar) direction with respect to the rotation axis as the pulsar spins down. Thus the MoI, and, consequently, the braking index, are both frequency dependent.

It is convenient to re-write (Eq. 2.5) as

$$\frac{d}{dt}\left(\frac{1}{2}I\Omega^2\right) = -C\Omega^4, \tag{2.10}$$

where $C = \frac{2}{3}R^6B^2sin^2\alpha$. Assuming this time that dI/dt and dC/dt are non-zero, differentiation of (Eq. 2.10) with respect to time gives

$$2I\dot{\Omega} + \Omega\dot{I} = -2C\Omega^3. \tag{2.11}$$

Differentiating once more gives

$$2I\ddot{\Omega} + 2\dot{\Omega}\dot{I} + \dot{\Omega}\dot{I} + \Omega\ddot{I} = -2\Omega^3\dot{C} - 6C\Omega^2\dot{\Omega}. \tag{2.12}$$

Using the chain rule we can write $\dot{I}$, and $\dot{C}$ in terms of $\dot{\Omega}$ and obtain

$$\dot{I} = I'\dot{\Omega} \tag{2.13}$$

$$\ddot{I} = \dot{\Omega}^2 I'' + I'\ddot{\Omega} \tag{2.14}$$

$$\dot{C} = C'\dot{\Omega}, \tag{2.15}$$

where the primed notation represents the derivatives with respect to Ω.

Substituting the identities shown above into (Eq. 2.11) and (Eq. 2.12), we get the following relations for $\dot{\Omega}$ and $\ddot{\Omega}$,

$$\dot{\Omega} = \frac{-2C\Omega^2}{(2I + \Omega I')} \tag{2.16}$$

$$\ddot{\Omega} = \frac{-\dot{\Omega}(2\Omega^3 C' + 6C\Omega^2) - \dot{\Omega}^2(3I' + \Omega I'')}{(2I + \Omega I').} \tag{2.17}$$

After some algebra, it is easy to show that the expression of the braking index as a function of angular velocity reads

$$n(\Omega) = \frac{\Omega\ddot{\Omega}}{\dot{\Omega}^2} = 3 - \frac{(3\Omega I' + \Omega^2 I'')}{(2I + \Omega I')} + \frac{C'\Omega}{C}. \tag{2.18}$$

We note that the magnetic dipole moment of the non-spherical pulsar may, in principle, also change with frequency. Estimation of this effect would require detailed

knowledge of the origin and distribution of the magnetohydrodynamics of the star, which is lacking. We therefore ignore such considerations here and restrict ourselves to analysis of the two effects described.

In the case of the MoI dominated high frequency regime, we hold C constant. We will return in the next chapter to this equation for the low frequency calculations in which we hold I constant, and allow C to change through migrating α as shown in Lyne et al. (2013).

2.3 Calculation method

It has so far been standard practice to adopt the canonical $1.4M_{\odot}$ with a radius ~ 10 km in calculations of the braking index. In this work, which includes frequency dependent MoI and varying M_B, we require the dynamic macro-properties of pulsars to be included in the calculation of the braking index. For this reason, it is necessary to employ physically realistic equations of state (EoS) in order to calculate the required neutron star properties. Rather than strictly use the canonical values, we employ calculated neutron star properties that are dependent on the structure of a particular EoS. In order to acquire the neutron star macro-properties, we solve the equations of motion of rotating stars with realistic EoS using two different numerical methods.

We test the modified braking index model using four physical EoS's. The EoS for neutron stars comes from essentially two main regimes; the high density core and the relatively low density crust. The EoS's from each region within the neutron star are calculated independently, and then connected continuously over the energy threshold between the two regions. In some cases, the cores of neutron stars can reach central densities of between 3 to 10 times the density of atomic nuclei. Ordinary nuclear matter consisting of nucleons and leptons is compressed so much under these conditions that exotic particles, such as heavy strange baryons and mesons may appear, and the occurrence of the hadron-quark phase transition cannot be excluded. For these reasons the EoS of the neutron star core is almost completely

unknown. In this work, we have chosen four EoS's which have been shown to reliably predict observed neutron star properties, and represent a reasonable approximation to behavior of high density matter.

2.3.1 The codes

The PRNS9 code, developed by Weber (1999, 2013), is based on a perturbative approach to rotation of spherical objects. Hartle and Thorne (1968) first approximated this effect using a perturbative expansion of the star's properties up to the second order in star's angular velocity, assuming a slow rotating star. In later work, a third order term in angular velocity has been included (Hartle and Thorne, 1973). The third order correction enters into the expression for the change of moment of inertia as a function of angular velocity (see Hartle and Thorne (1973)) studied in this work. This approximation was implemented by Weber, with the addition of self-consistency conditions, in the PRNS9 code.

To ensure the reliability of the PRNS9 code results, we also used the RPN code. This code by Rodrigo Negreiros (Negreiros, 2012) is based on a publicly available algorithm, RNS, developed by Stergioulas and J. L. Friedman (1995). The equations of motion are derived directly from Einstein's equations, following the Cook, Shapiro, and Teukolsky approach (Cook et al., 1992), described in detail in Komatsu et al. (1989). Both codes are applicable to stars rotating with all frequencies up to the Kepler limit.

A comparison of the results of the two codes is demonstrated in Figure 2.1 which shows MoI as a function of frequency for a pulsar with the QMC700 EoS and M_B = 2.0 $M_\odot$ (see Section 2.3.2). They differ most, but by less than 10%, as the Kepler frequency is approached. This difference has no consequence in practical application as no pulsars are known to rotate near Kepler frequencies, and we can assume all pulsars considered here are rotating well below their mass shedding limit (see Table 2.1 for EoS and M_B used in this paper). The small difference at near zero frequency

(about 1.25%), due to the difference in behavior of the two low density EoS's (see Section 2.3.2), is negligible in the context of calculating the neutron star macro-properties used in this work.

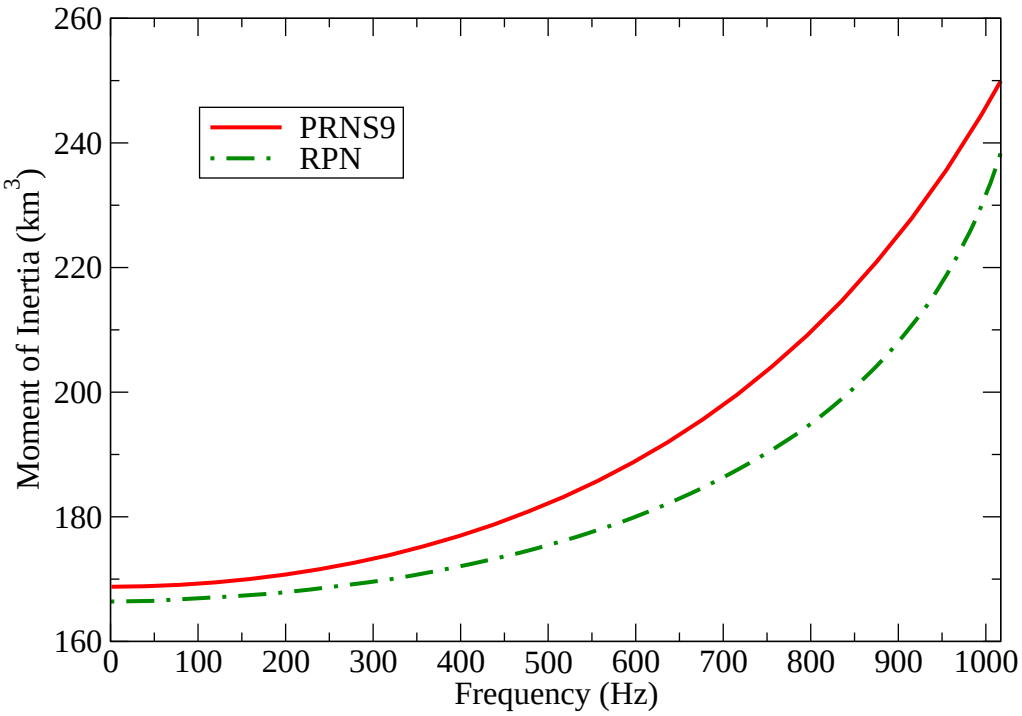

Figure 2.1: (Color on-line) MoI as a function of frequency for a pulsar with M_B = 2.0 $M_\odot$ as calculated with both RPN and PRNS9 numerical codes.

Unless stated otherwise, we present the PRNS9 code results as this code has an output that is set up to readily provide calculation results of some observables that are needed in our study (see Sec 2.4), data not initially available in the RPN code output. This choice is purely for convenience of generating informative plots easily from the data.

Table 2.1: Kepler frequencies in Hz for EoS's and $M_B/M_\odot$ used in this work.

EoS/M_B	1.0	1.5	2.0	2.2
KDE0v1	820	1024	1230	1327
NRAPR	778	985	1198	1312
QMC700	745	888	1017	1070
HV	612	761	908	985

2.3.2 The Equation of State

An essential input to the calculation of macroscopic properties of rotating neutron stars is the EoS. The EoS is constructed for two physically different regimes, the high density core (composed of uniform nuclear matter) and the relatively low density crust (composed of nuclei). Each EoS, representing the two regions, is constructed independently, and then smoothly matched over the threshold density marking the transition from crust to core.

The microscopic composition of high density matter in the cores of neutron stars is not well understood. We have chosen two EoS, which assume that the core is made of uniform nuclear matter consisting of nucleons only, KDE0v1 (Agrawal et al., 2005) and NRAPR (Steiner et al., 2005). These EoS were selected by Dutra et al. (2012) as being among the very few which satisfied an extensive set of experimental and observational constraints on properties of high density matter. Dutra *et al.* tested 240 parameterizations of the non-relativistic effective Skyrme interactions for their performance in predicting various properties of nuclear matter. They found that only a small set of the parameterizations satisfied all the known experimental and observational constraints. Strictly speaking the Skyrme effective interaction is a low momentum expansion of the nuclear force and may be questionable at densities higher than about 3 times nuclear saturation density. However, some of the neutron star models used in this work have low maximum masses and it is possible that the central densities do not exceed the limit of validity of the Skyrme force. In addition to the nucleon-only EoS, we use two other realistic EoS which include the heavy strange baryons (hyperons) as well as nucleons. The QMC700 EoS is derived in the framework

of the Quark-Meson-Coupling (QMC) model (Guichon et al., 2006; Stone et al., 2007), and the Hartree V (HV) EoS (Weber and Weigel, 1989) is based on a relativistic mean-field theory of nuclear forces.

The maximum mass of a static star, calculated using the Tolman-Oppenheimer-Volkoff (TOV) equation, is 1.96, 1.93, 1.98, and 1.98 $M_\odot$ for KDE0v1, NRAPR, QMC700, and HV, respectively, which is close to the gravitational mass of the heaviest known neutron stars (Demorest et al., 2010; Antoniadis et al., 2013). The EoS are illustrated in Figure 2.2, which shows pressure as a function of energy density ϵ in units of nuclear saturation energy density $\epsilon_0 = 140$ MeV/fm^3. We observe that the pressure increases as a function of energy density almost monotonically for KDE0v1, NRAPR, and HV, whereas QMC700 EoS predicts a change in the rate of increase at about 4 ϵ_0. This change, and the subsequent softening of the EoS, happens at the transition energy density marking the threshold for the appearance of hyperons in the matter. Such a change is not apparent in the HV EoS. The main reason for the difference between the two hyperonic models is that the QMC700 distinguishes between the nucleon-nucleon and nucleon-hyperon interactions (neglecting the poorly known hyperon-hyperon interaction), whereas the HV model uses a universal set of parameters for all hadrons. Inclusion of both the QMC700 and HV EoS in this work reflects the uncertainty in the theory of dense matter in the cores of neutron stars.

The high density EoS (KDE0v1, NRAPR, HV and QMC700) are smoothly matched to the low density EoS at the threshold near nuclear energy density. For the different numerical codes, it was necessary to use slightly different low density EoS. For the RPN neutron star models, the low density EoS is given by Baym-Bethe-Pethick (see Baym et al. (1971a) and Table 5 in Baym et al. (1971b)) at about 0.1 fm^{-3}, augmented by Baym-Pethick-Sutherland (Baym et al., 1971b) at about 0.0001 fm^{-3}, going down to $\sim 6.0\times\ 10^{-12}$ fm^{-3}. For the PRNS9 neutron star models, the EoS is matched to the Harrison-Wheeler (Harrison and Wheeler, 1965), taken for the outer crust of the star, and Negele-Vautherin (Negele and Vautherin, 1973) equation of state for the inner crust. The reason for this difference is purely a matter of easing

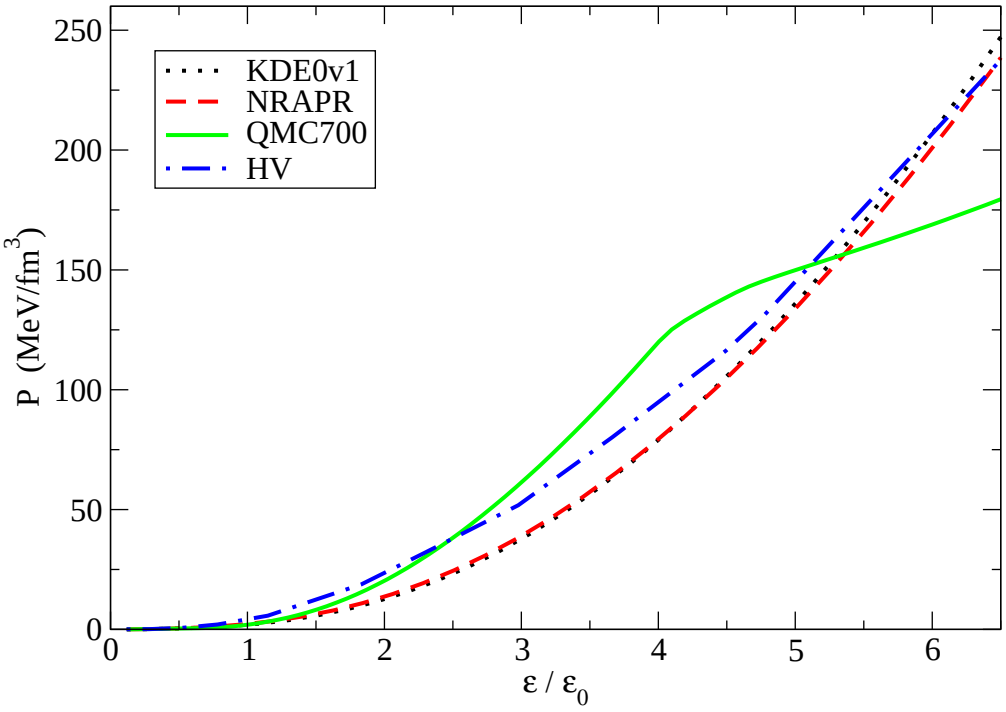

Figure 2.2: (Color on-line) Pressure vs energy density ϵ (in units of the energy density of symmetric nuclear matter at saturation ϵ_0) as predicted by the four EoS's used in this work.

the numerical calculations within the architecture of each code, and the neutron star macro-properties are not affected by these different low density EoS in the context of the present work.

2.4 Results and discussion

As detailed in the previous section, the calculation of the value of the braking index as a function of frequency has been done for a multiple combination of codes, EoS, baryonic masses, and changing I of the rotating star. We have also included an effect that mimics possible superfluid conditions thought to exist in the inner crust and core of the star. In this section, we illustrate our findings by showing typical representative results, and discuss some deviation from them if appropriate. Unless stated otherwise, the example EoS used in the figures is arbitrarily chosen to be QMC700, and the neutron star modeling code in use is PRNS9.

2.4.1 Braking index with frequency dependent MoI

Figure 2.3 shows the braking index as a function of frequency as calculated in the derivation introduced in Section 2.2.1 where C is considered to be constant. The braking index curve deviates from the canonical value of $n = 3$ as a function of frequency. From the curve, we see that deviation from $n = 3$ is highest toward Kepler frequency, and approaches the value of three at low frequency.

As part of the attempt to realize the full range of the dynamical braking index, we looked systematically at the contribution by each individual EoS. Figure 2.4 gives an example of the braking curve, as calculated by using PRNS9 code for a star with 2.0 $M_\odot$ baryonic mass. When Figure 2.4 and Figure 2.2 are compared side-by-side, a clear correlation between EoS stiffness, and braking index curve can be seen. Softer EoS's yield a lower braking index as a function of frequency, but also only support lower mass objects as a function of central energy density. The softer EoS, by definition,

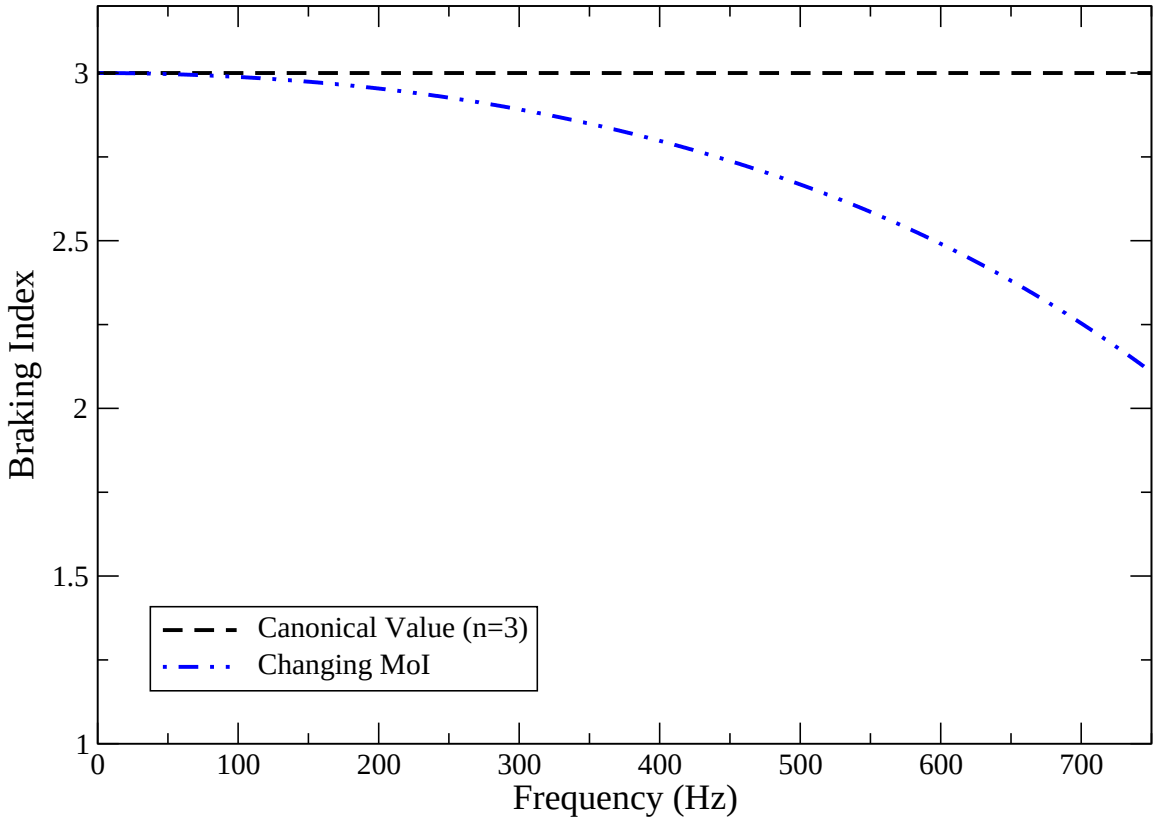

Figure 2.3: (Color on-line) Braking index as a function of frequency calculated using the PRNS9 code, for a pulsar of 2.0 $M_{\odot}$ baryonic mass with the QMC700 EoS with C constant (see text for more explanation).

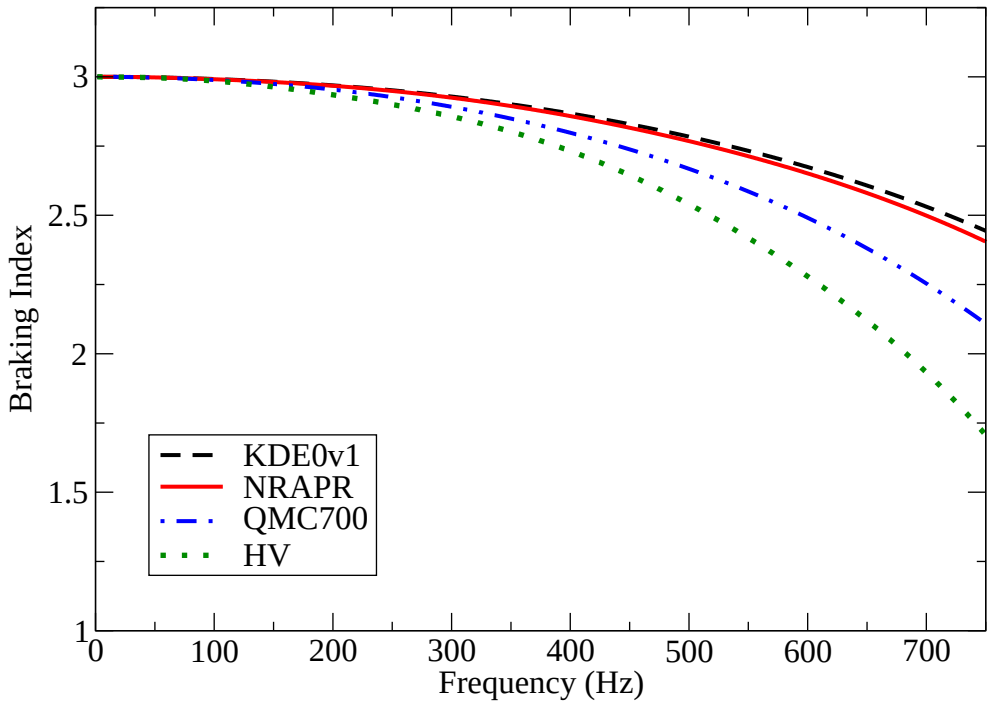

Figure 2.4: (Color on-line) Braking index as a function of frequency calculated for a pulsar with $M_B = 2.0\ M_\odot$ with all EoS's adopted in this work.

has less response in pressure for increasing density, thus the star is more deformable, but supports less mass against gravitational collapse.

Another important aspect of this study results from varying the rest mass of pulsars in the calculations. For each EoS, and for all dynamic conditions, we have tested a range of baryonic rest mass. The effect of varying mass for a single EoS calculated in the PRNS9 code is shown in Figure 2.5. The braking index range is related to rest mass in that the lowest mass pulsars see the largest change as a function of frequency. In order to show the full extent that the braking curve changes with frequency, we started at a relatively high baryonic mass of 2.2 $M_\odot$, which represents a roughly 2.0 $M_\odot$ (gravitational mass) neutron star, and tested our model down to

1.0 $M_\odot$ baryonic mass, which represents an object with a central energy density close to that of normal nuclear matter, and very low mass. This range of masses covers the mass spectrum of known neutron star observations, and is consistent with the limits on mass in neutron star theory (limited, in the upper region, by the physical EoS, and in the lower region by the stellar evolution that resuts in the neutron star).

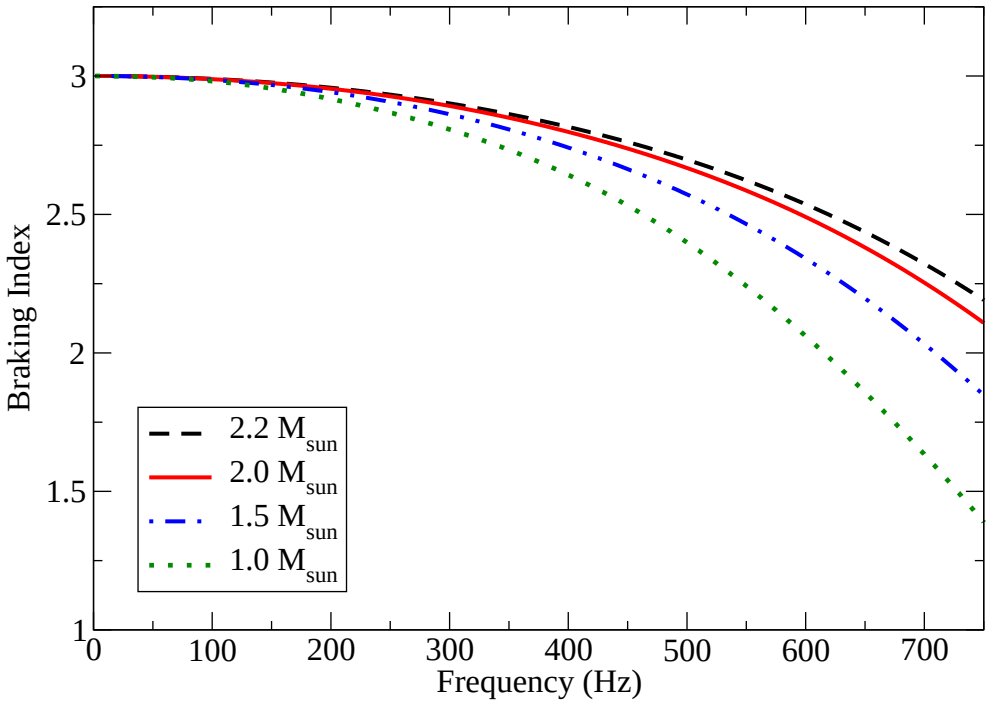

Figure 2.5: (Color on-line) Braking index as a function of frequency calculated of pulsars with M_B = 1.0 - 2.2 $M_\odot$.

As a general feature, we find that any appreciable deviation of the braking index from the generic value $n = 3$ is observed only at rotational frequencies higher than about 250 Hz. The sensitivity of this deviation to the EoS and M_B is demonstrated in Figures 2.4–2.5. As can be seen in Figure 2.4, the biggest change in the braking index of an M_B = 2.0 $M_\odot$ pulsar is predicted by the HV EoS, followed by the QMC700,

reaching $\sim$ values 1.75 and 2.15 at 750 Hz, respectively. The two nucleon-only EoS, KDE0v1 and NRAPR, behave in a very similar way and predict a larger value of ($n = 2.5$) at this frequency. These trends can be directly related to the properties of the EoS. Figure 2.5 shows the sensitivity to M_B for the QMC700 EoS. The effect clearly increases with decreasing M_B.

We recall that the stiffness/softness of the EoS relates to the rate of change of pressure with changing energy density ϵ. For each EoS, the frequency dependent ϵ is given in Table 2.2. Using Figure 2.2 we obtain the corresponding pressures. Figure 2.6 plots the pressure vs ϵ relation for each EoS, the slope indicating the stiffness/softness in each case. The maximum change in the braking index in Fig. 2.4, observed for the HV EoS, is seen to be associated with the smallest change in pressure with increasing ϵ, i.e., the largest softness. The stiffest EoS, KDE0v1 and NRAPR, predict the smallest response to the pulsar's rotational deformation. This conclusion is further supported by results shown in Figure 2.5. Pulsars with the lowest M_B, governed by the softest EoS, exhibit the largest change in the braking index at high frequency. The deformation of the star, governed by EoS stiffness and stellar mass, is discussed in greater detail in 2.4.2.

2.4.2 Superfluidity

The effects demonstrated in Figures 2.4–2.5 were calculated assuming that the whole body of a pulsar contributes to the total (core+crust) MoI. However, some theories suggest the conditions inside a pulsar are consistent with the presence of superfluid/superconducting matter, both in the crust and in the core (Sedrakian and Cordes, 1998; Ho and Andersson, 2012; Page et al., 2014; Hooker et al., 2013). Superfluid material would not contribute to the change in rotation of the star thus reducing the MoI.

In this work, we consider an extreme case in which the whole contribution of the core to the total MoI is removed. This scenario could be realized, for example, if either

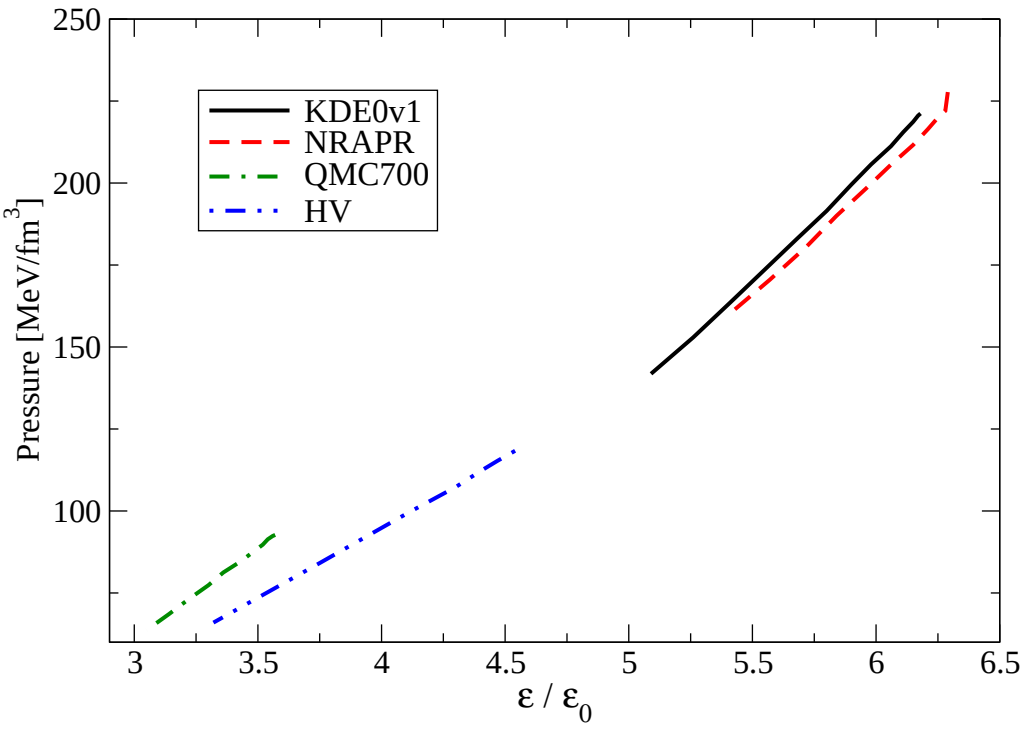

Figure 2.6: (Color on-line) Pressure as a function central density of a pulsar with $M_B = 2.0\ M_\odot$, rotating with frequencies decreasing from the Kepler limit to zero as predicted by the four EoS's used in this work. Relation between the central density and frequency is given in Table 1.1. For more explanation see the text.

Table 2.2: Central energy density (in units of the ϵ_0) of a pulsar with HV, QMC700, NRAPR, KDE0v1 EoS and $M_B = 2.0\ M_\odot$ as a function of decreasing rotational frequency. For more explanation see text.

Frequency [Hz]	HV	QMC700	NRAPR	KDE0v1
1200	–	–	5.04	5.09
1100	–	–	5.23	5.26
1000	–	3.05	5.40	5.41
900	3.32	3.14	5.57	5.55
800	3.54	3.22	5.72	5.68
700	3.75	3.30	5.84	5.80
600	3.94	3.36	5.96	5.90
500	4.11	3.43	6.06	5.98
400	4.30	3.48	6.15	6.06
300	4.40	3.52	6.21	6.11
200	4.47	3.54	6.25	6.15
100	4.52	3.56	6.28	6.17
0	4.54	3.57	6.29	6.18

the whole core is superfluid, or there is a layer of superfluid material between the core and the inner crust of the star, preventing any angular momentum transfer between the core and the crust. Either scenario simply results in removal of the contribution of the core to the MoI. To model this effect, it was necessary to locate the transition between the two phases of neutron star matter, which is assumed to occur roughly at 120 MeV/fm^3. The corresponding pressure is dependent on the EoS and is used to locate the physical position of the transition along the polar and equatorial radii. The results are schematically illustrated in Figure 2.7, which shows the proportion of the core (equatorial) radius in a static star and a star rotating at an arbitrarily chosen frequency of 600 Hz as a function of M_B, as predicted by the KDE0v1 EoS. We observe that the proportion is different for a static and rotating star, mainly because of the varying shape of the star. The expansion (compression) along the equatorial (polar) direction with respect to the rotational axis leads to larger deformation of the less dense crust than that of the denser core.

It is worth looking into the frequency dependent changes in crust/core behavior of the pulsars which explains the result in Figure 2.7. For each individual star, the

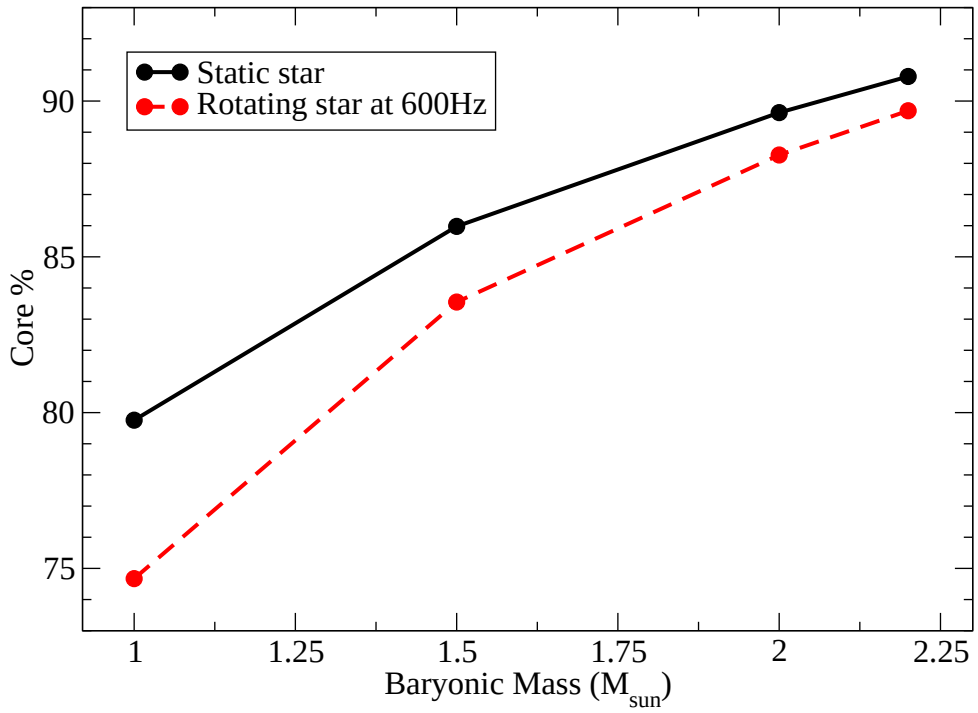

Figure 2.7: (Color on-line) Percentage of the core in a static star (by mass) and a star rotating at 600 Hz as a function of M_B. For more explanation see the text.

total ratio of crust/core material is governed by the EoS and the baryonic mass. For a given EoS, the radial percent of core in the star goes up as mass increases, and for a given mass, the percent increases with increasing stiffness of the EoS. The relative pressures of each EoS at each given mass dictates the transition energy where the crust and core regions meet. For example, the relatively soft HV EoS transitions from crust to core at higher pressure than the others, thus resulting in a transition deeper within the star. The remaining EoS are similar in behavior at low density, but the softening of the QMC700 EoS is evident at the higher masses where the onset of hyperons starts to soften the EoS. The initial crust/core ratio of a given pulsar is very important to the effects of removal of the core from MoI. As the star rotates, we find

that the crust deforms significantly more than the core. Therefore, stars with larger fractions of their mass in the core see less overall deformation and a larger effect from core removal, and stars with less massive cores see more overall deformation and a noticeably smaller effect of core removal.

We calculate the ratio of core to crust material along the radius of the star. We make the assumption that nuclear saturation density is roughly 120 MeV/fm^3, and that this represents the transition from ordinary nuclear matter in the crust to the super-dense core. A close view of the EoS, near this transition density, is shown in Figure 2.8 where we can see the relative differences in pressure at the crust/core interface (120 MeV). Each EoS has a corresponding pressure at the given energy density which represents a position, in the star, along the radius. In this way we are able to estimate the physical position within the star, along the radius, where the core ends and the crust begins. This position, dependent on the mass of the star and the EoS, is initially calculated for a static star which is then allowed to rotate to arbitrary frequencies, and calculated again. The results of this calculation are described below.

Figure 2.9 shows the percentage of core in non-rotating neutron stars by mass for each EoS. From the figure it is clear that the higher mass objects have a much higher percentage of core material versus crust, and this is to be expected. There exists a lower limit for rest mass below which the entire star will consist of crust material, though it is uncertain if neutron stars of this low mass can be formed, and the star approaches some upper limit where it consists mostly of core material at higher mass.

A plot of the evolution of the percentage of core material along the polar and equatorial radii, by comparison, is shown in Figure 2.10, using the HV EoS. It is clear that most of the change in the percentage of core material occurs equatorially. The polar composition by radius remains *relatively* constant. This implies that while the total polar radius shrinks with rotation, this change occurs predominatly in the crust rather than in the core. This is consistent with the equatorial radial change which gets larger with rotation, and most of the increase comes in the crust. We see that

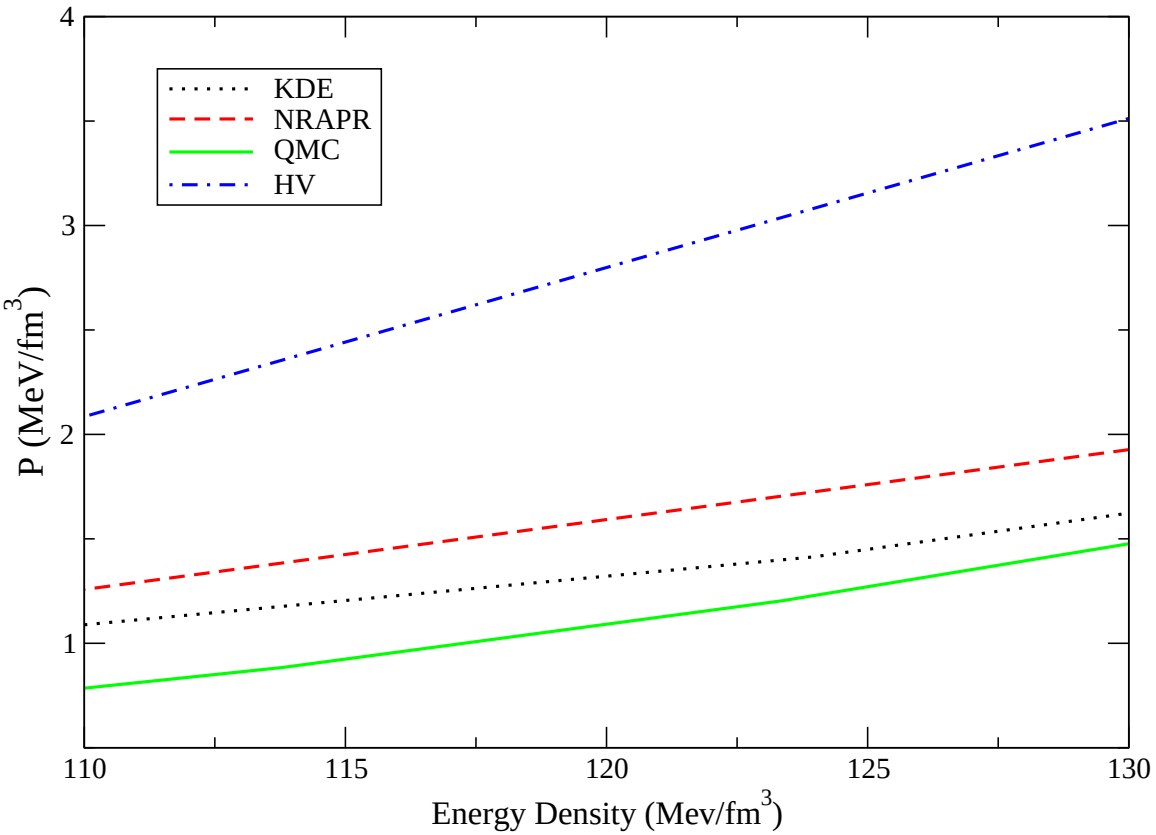

Figure 2.8: The four physical EoS's used in this study. We show the behavior of each EoS around the crust/core transition density of 120 MeV/fm^3.

the star gets more oblate with rotation as seen from the surface, but the core remains *essentially* spherical.

What can be taken from Figures 2.9, and 2.10 is that when the star spins up, the percentage of core material along the radial axis decreases slightly. This decrease is more significant at lower masses. Physically, rotation provides effective pressure which reduces density and hence mass in the nuclear matter region while the star is deformed from a (static) sphere. As the equatorial radius gets larger, the portion of radius that is core material is not increasing as fast as the total star, and hence there is more crust material, so the percentage of core is reduced. At higher mass, the initial percentage of core is much higher, and the effects of rotation are less significant in terms of increasing crust material along the equator. We see that the crust material deforms much more readily than the core.

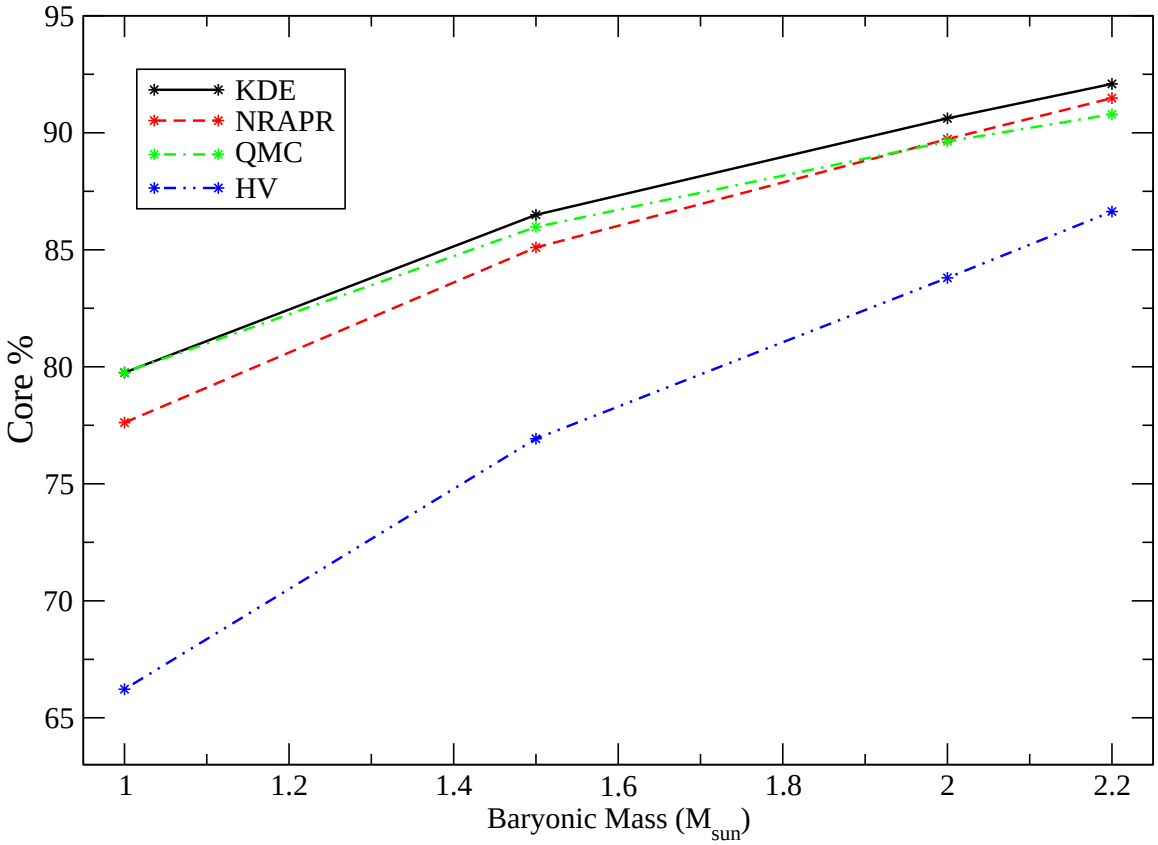

Figure 2.9: Percent of star that is core material by mass for non-rotating stars.

The deformation of the star away from spherical, for the arbitrarily chosen frequency of 600Hz, is shown in Figure 2.11. It is clear that the lowest mass stars see the highest amount of surface deformation at a given frequency. The deformation clearly relates to the percent of core material as shown in Figure 2.9. At a given frequency, we can conclude that the stars with the highest amount of crust material by percentage will see significantly more deformation than stars with the highest amount of core material by percentage.

The percentage reduction in moment of inertia by mass is illustrative of the crust/core relation. From the preceding data, we see that the stars with the lowest amount of core material are more deformed at lower frequencies than their high percentage core counterparts. In removing the core from the contribution to angular momentum, we see this difference manifest in two ways. For lighter stars, with a lower

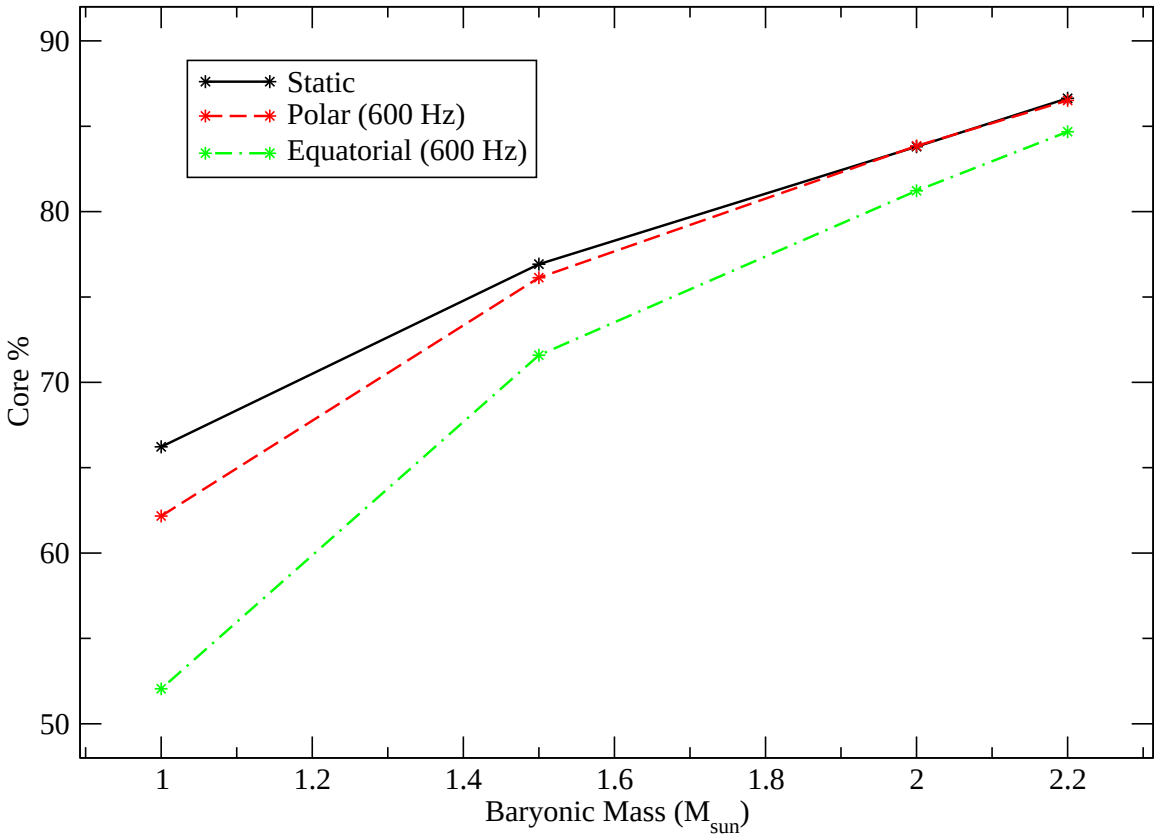

Figure 2.10: Percent of star that is core material by mass comparison between static, and rotating models where both polar and equatorial radius are considered.

percent of core material, there is larger deformation due to the higher amount of crust material, and the removal of the core has less impact on the total mass. Therefore, the reduction of moment of inertia is less. Conversely, the higher mass stars, with a high percentage of core material, will deform less at the same frequency, and the removal of the core has a high impact on the reduction of total mass contributing to angular momentum. From these considerations, it is clear that the removal of the core, at a given frequency, will reduce the moment of inertia much more significantly for stars with higher masses, although the reduction of braking index, due to changes in MoI, is less significant for heavy stars than for light ones.

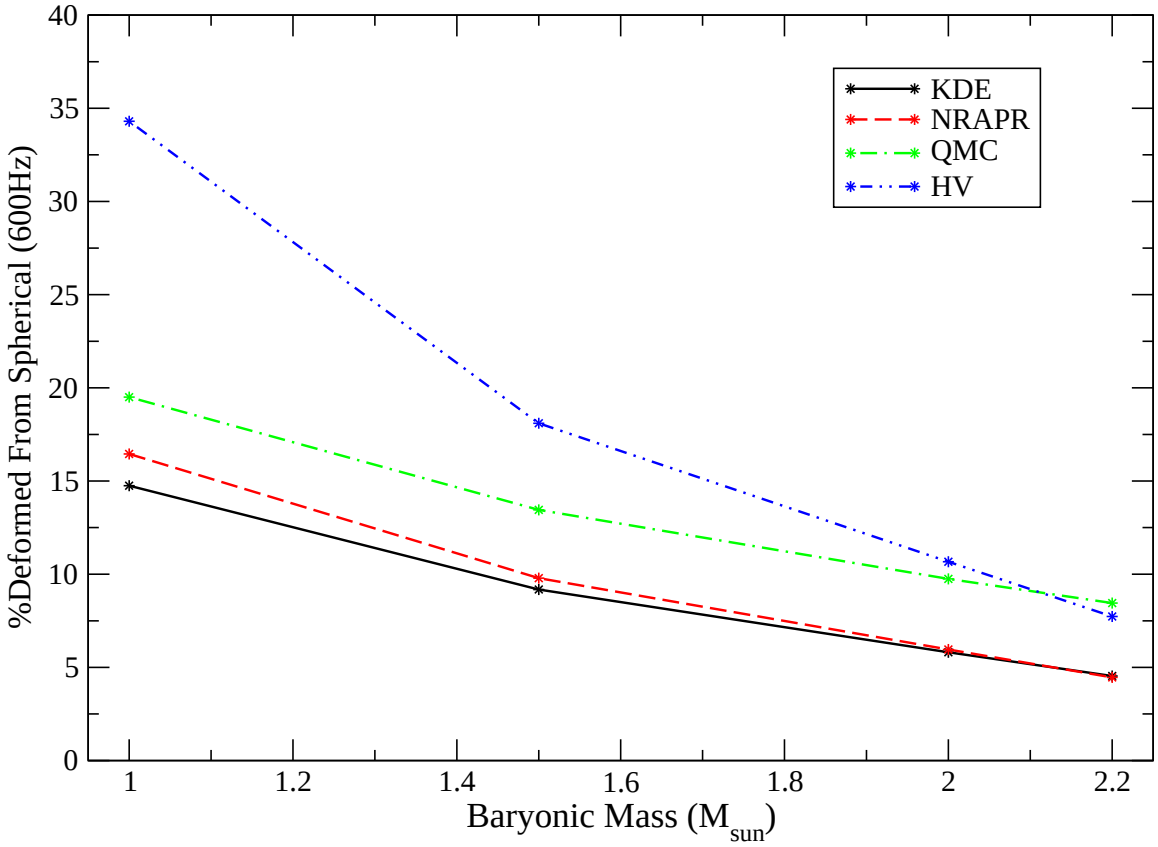

Figure 2.11: Percent of deformation away from spherical at 600Hz.

2.4.3 Core elimination

As stated above, we have included a phenomenological superfluid effect in order to further reduce the braking index curve, where there exists a latent portion of superfluid material in the inner crust of neutron stars that does not contribute to the moment of inertia, and hence acts as an angular momentum reservoir. Assuming this is the case, or that there is some amount of superfluidity in the core, we consider an extreme version of this effect where there exists a superfluid barrier in the crust/core region which disallows the exchange of angular momentum. In this case, the MoI is modeled for the crust only, effectively lowering the overall I as a function of frequency. We see in Figure 2.12 an example for a single modeled EoS, at a given constant baryon

mass, where we see two curves for moment of inertia. The solid line is our original calculation, and the dashed line is a calculation of only the moment of inertia coming from the crust, where we are effectively allowing no momentum exchange between the crust and core of the star.

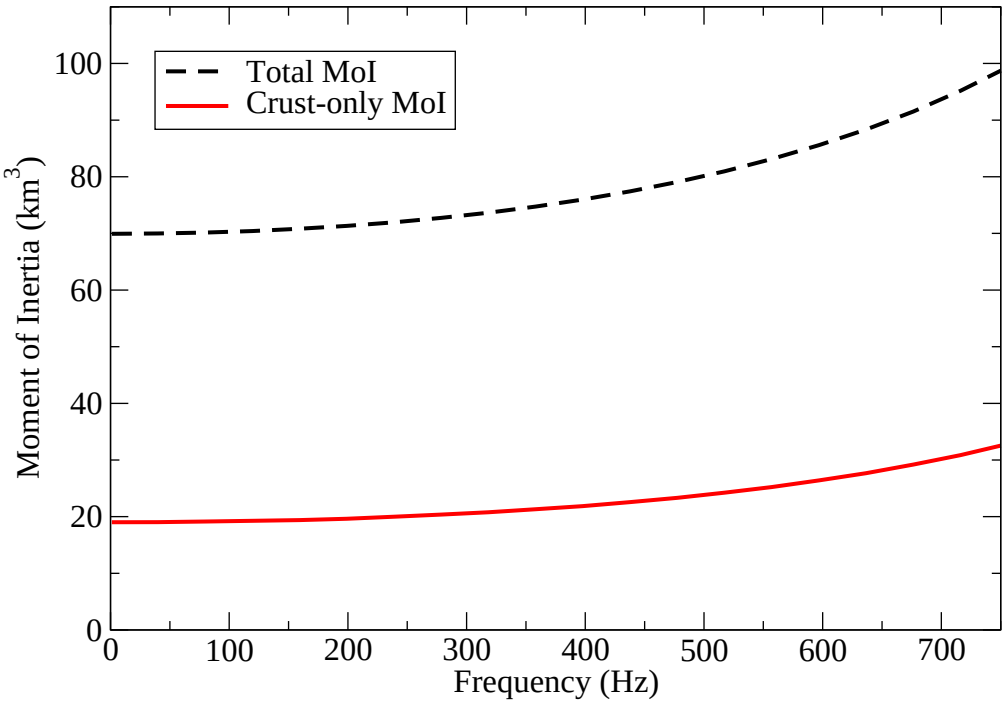

Figure 2.12: (Color on-line) Total (crust and core) and the crust-only MoI as a function of frequency, calculated for a pulsar with $M_B = 1.0\ M_\odot$.

In Figure 2.13, we have an example of how the imposed superfluid condition reduces the braking index curves in this work. We illustrate here the effects of reducing the baryonic mass, and then the further reduction that comes from the imposition of the superfluid effect. The highest overall effect comes from the smallest mass pulsars in this study because of the reasons described above. It should be noted that the reduction of the braking index of the crusty-only $2.2M_\odot$ star falls very close to the

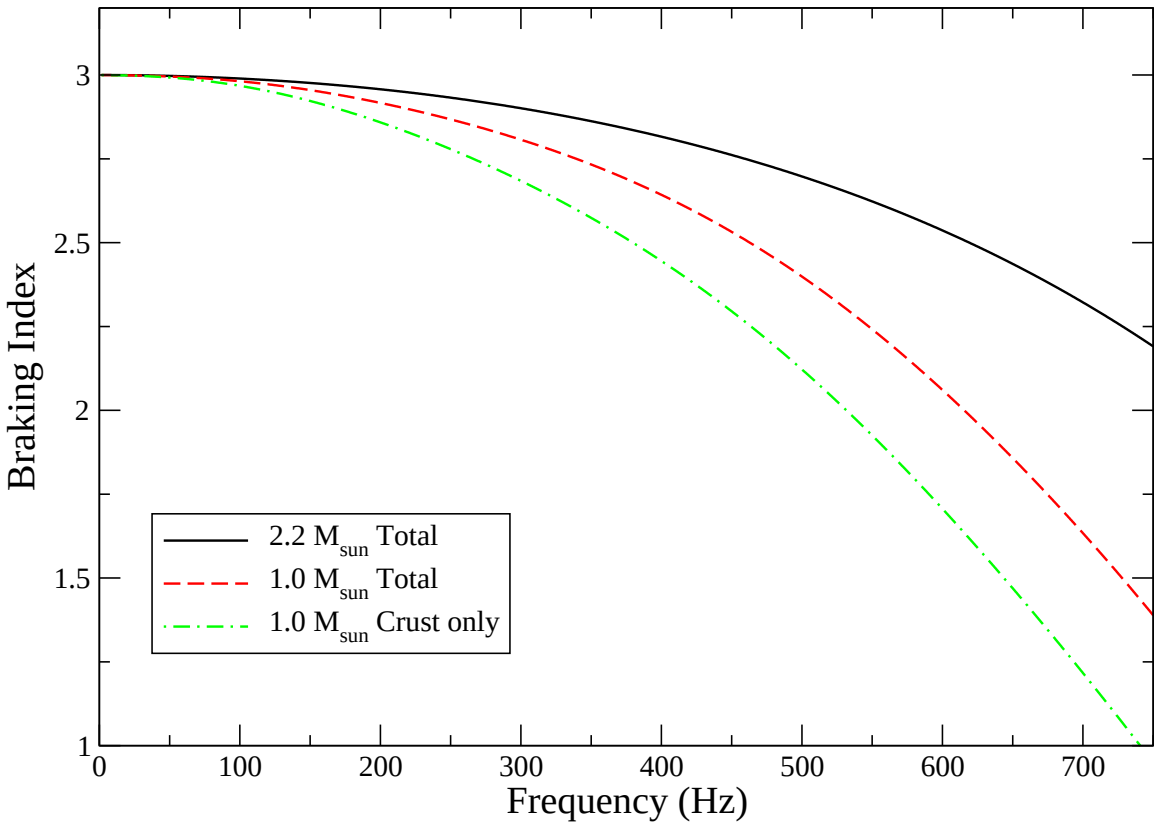

Figure 2.13: (Color on-line) We show here the effect of eliminating the core angular momentum from the calculation for the simulated superfluid condition. This effect is insignificant below about 150 Hz.

$1.0M_{\odot}$ line with total MoI. Thus the overall deviation in braking is largest for the small mass star, the relative reduction is larger for the high mass star as predicted above.

We represent in Figure 2.14 the resulting braking index curves obtained, for a single EoS (QMC700) at a given constant baryon mass, with changing MoI and the simulated superfluid effect. From Figure 2.14, it should be clear how each step reduces the curve to lower values. This lower limit provides the boundary for the full range of braking index as a function of frequency while keeping the inclination angle α, and magnetic field strength constant.

Elimination of the core contribution can lead to a dramatic lowering of the total MoI by more than a factor of three, as shown, for example, in Figure 2.12 for the

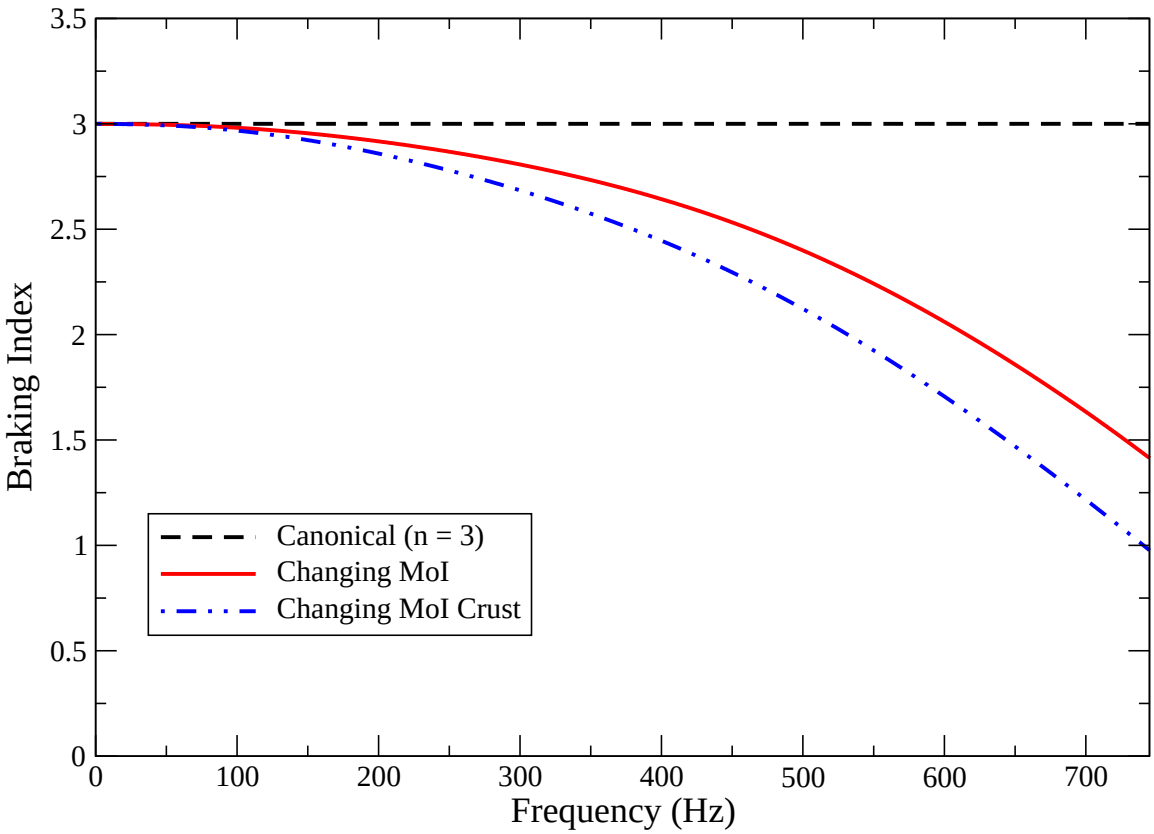

Figure 2.14: (Color on-line) Braking index as a function of frequency calculated with PRNS9 code and QMC700 EoS for a neutron star with 1.0 $M_{\odot}$ baryonic mass. This is similar to Figure 2.3, but now with the inclusion of the curve with the core angular momentum removed.

1.0 $M_{\odot}$ baryon mass and the QMC700 EoS. The difference between the total and crust-only MoI shows a weak frequency dependence with a slight increase above roughly 600 Hz. In turn, the reduction of the MoI by removal of the core contribution leads to additional changes in the braking index on top of the changes due to the frequency dependent MoI (see Figure 2.5) as shown in Figure 2.15. This change is, as expected, larger for higher mass stars that contain a more significant proportion of dense core material than for lower mass stars that are more crust-like throughout.

For the purpose of this work, we assumed that there is sufficient superfluid material located in the transition region between the crust and core of the star to disallow exchange of angular momentum, but made no assumption as to the superfluidity (or

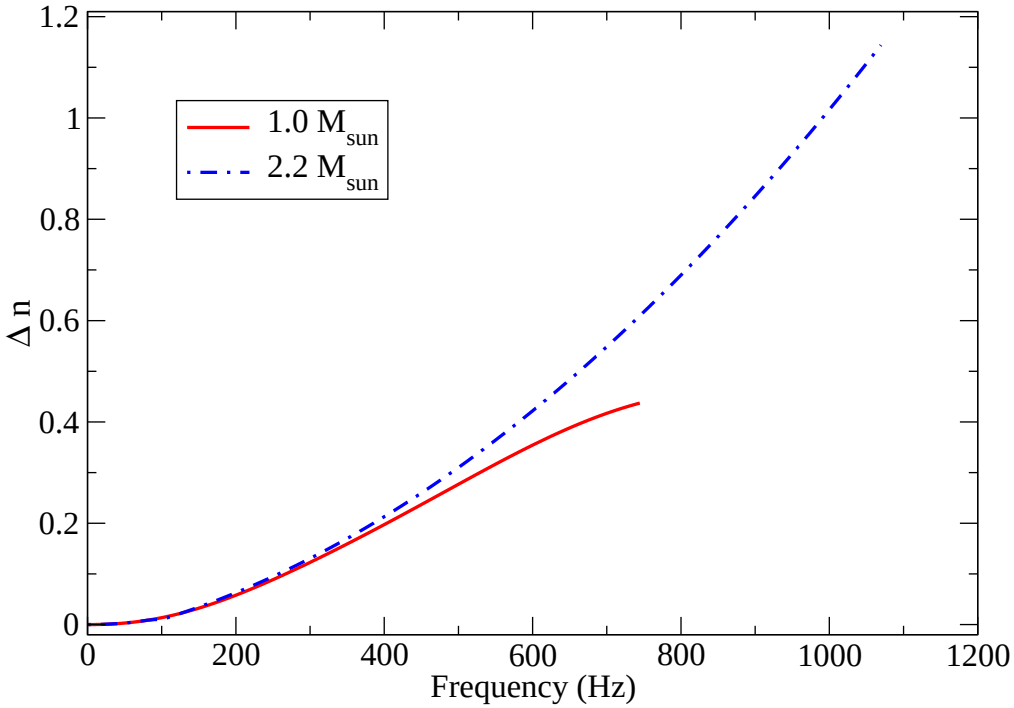

Figure 2.15: (Color on-line). Δ n represents the difference in braking index as a function of frequency between stars with (see Fig. 2.5) and without core contribution to the MoI. Each curve is displayed up to the Kepler frequency of the star.

not) of the neutron star as a whole. The effects reported here should be taken as illustrative rather than definitive of the possible effects of superfluidity.

2.5 Summary

The variation of the braking index of isolated rotating neutron stars of mass M_B = 1.0, 1.5, 2.0, and 2.2 $M_\odot$ with rotational frequency from zero to the Kepler limit within the MDR model with frequency dependent MoI has been investigated. The microphysics of the star was included through utilizing realistic EoS of the pulsar

matter. An illustration of the possible effect of superfluidity in the star core has been included in the study.

Compiling the models constructed from every condition that can change the MoI as explained above, along with the simulated superfluid condition, we get a definitive range on the braking index curve as a function of frequency. The maximum change in the braking index is obtained with the QMC700 EoS and 1.0 $M_\odot$; the least effect is found for KDE0v1 at 2.2 $M_\odot$. Figure 2.16 represents the upper and lower braking index curves achieved by our model for both numerical neutron star codes. The lower limit is the result of allowing a changing MoI, for the softest equation of state, at the lowest mass, including the phenomenological superfluid effect, while keeping the surface magnetic field strength and inclination angle constant. What results from our calculations is a braking index curve that is relatively much lower than the one described by a simple dipole torque acting with static properties on a canonical mass neutron star. However, this reduction is realized only at frequencies that are some significant fraction of Kepler frequency, and/or at very low M_B. At frequencies closer to those observed for pulsars with a well documented braking index, the reduction away from $n = 3$ is negligible (see Chapter 3).

The conditions used so far in this study have reduced the braking index significantly from the canonical value of $n = 3$, but, as expected, have failed to accurately model known observations as stated above. Most of the effects explored have a large effect only at the high frequencies usually associated with very young, or binary pulsars, and do not recreate the observed conditions of braking index for isolated pulsars rotating at low frequencies. The conditions used thus far show the effects of rotational dynamics on MDR braking index, but all reliable observations are seen at low frequencies where the effects are negligible. While agreement with observation is strictly not met, we gain some insight into the high frequency behavior of braking index in the MDR model.

In order to show the importance of an additional changing variable in the MDR model, we calculate the amount of deformation in the rotating star, and plot it

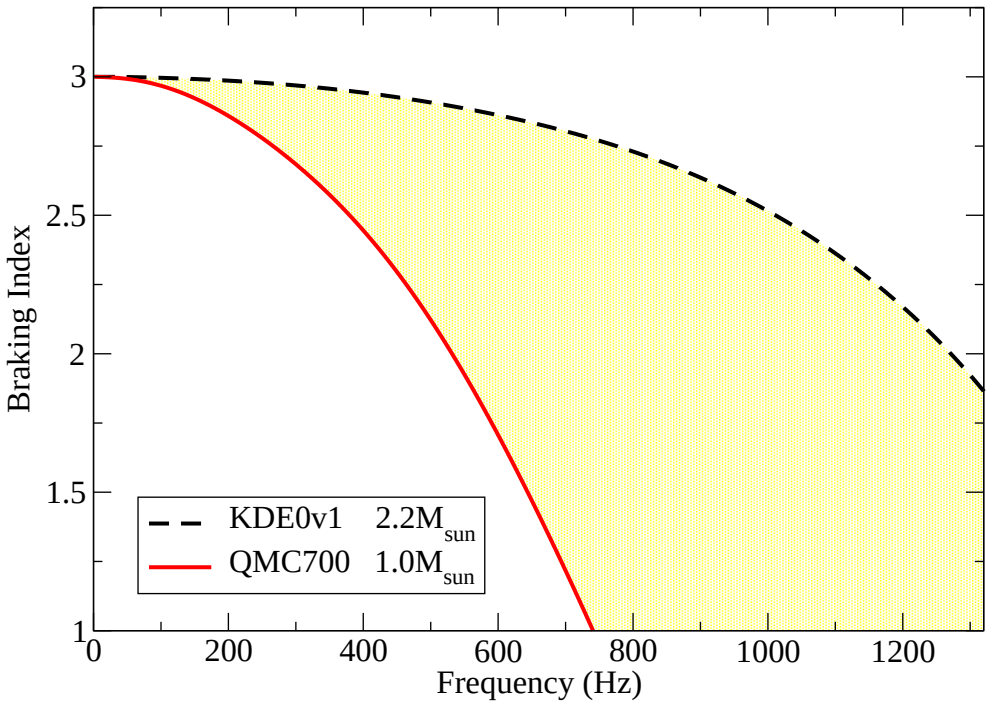

Figure 2.16: (Color on-line) Lower and upper limits on values of the braking index as a function of frequency, including results from both numerical codes, all EoS's, M_B, and the superfluid condition. The (yellow) shaded area between the two lines defines the location of all results within the limits. The pulsar with baryonic M_B = 2.2 $M_\odot$ and the KDE0v1 EoS has the highest Kepler frequency (see Table 2.2) and defines the frequency limit in this work.

(normalized to 3 for comparison) along side the changing braking index as a function of frequency in Figure 2.17. We see that over a range of about 150 Hz, the star remains spherical within about 1.2%, while the braking index stays within about 2% of the canonical value, $n = 3$. This is important for two reasons. First, the MDR model is based on a spherical object, and large deformation should complicate the magnetic field. Second, we see that the changing MoI in the MDR model has negligible effect at this range of frequency which is also much higher than the frequencies seen in the reliable observations shown in Table 1.1.

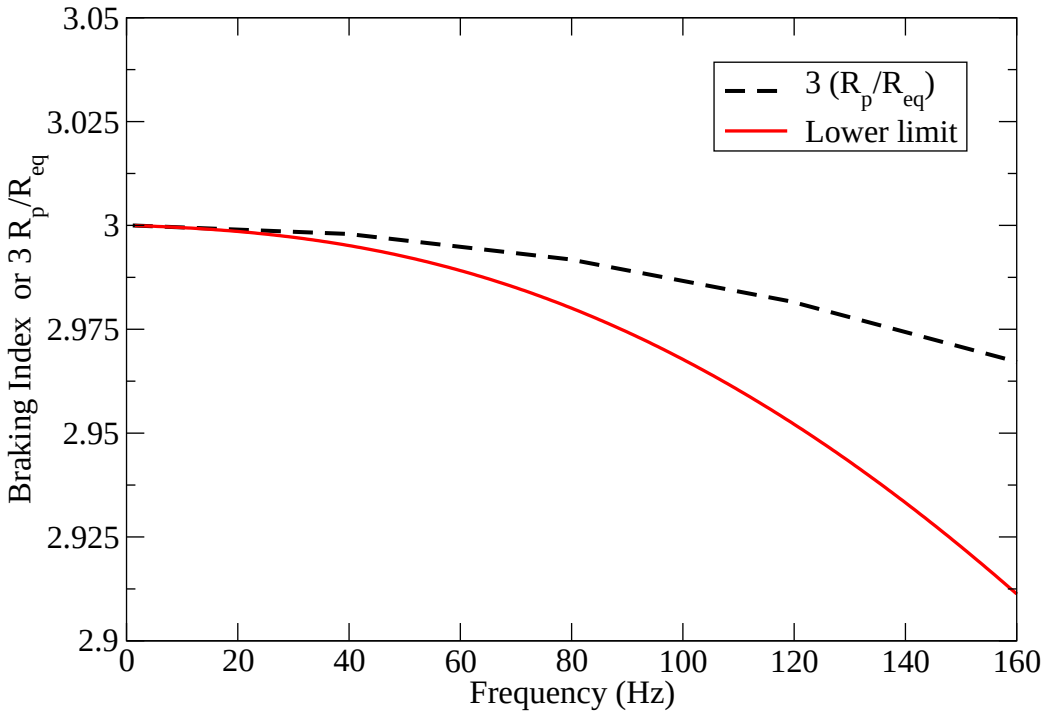

Figure 2.17: (Color on-line) The lower limit of the braking index (see Figure 2.16) as a function of frequency (solid line) compared with the ratio between polar (R_p) and equatorial radii (R_{eq}), normalized to three, which determines deformation of the star. The difference between the two lines represents a correlation between deviations of the braking index from $n = 3$ and deformation for a 1.0 $M_\odot$ pulsar rotating at frequencies below 160 Hz (notice the expanded y-scale). It is seen that the shape deformation, even for this most deformable star, is small at these frequencies and quite unable to reproduce the observed range of braking indices.

2.6 Conclusions and outlook

We calculated models of the braking index of rotating neutron stars with constant baryonic mass within the framework of the MDR assumption. We allowed rotational frequencies from zero to the specific Kepler frequency defined from the central energy density of each tested pulsar. We used four different, physically realistic, EoS, two different numerical codes, and the baryonic rest mass was set over the range of $M_B =$ 1.0 $M_\odot$ – 2.2 $M_\odot$. We calculated properties of the rotating star as functions of frequency, and used this data to calculate the braking index as a function of frequency in an attempt to examine the full range of the dynamical braking index.

At frequencies in the range of reliable pulsar braking index observations, our dynamical study shows that the canonical value of $n = 3$ prevails in the framework of MDR. Our results show the largest deviation from $n = 3$ at frequencies approaching a significant fraction of Kepler frequency for all model improvements which maintain constant α and magnetic field strength. These results show a very high dependence on the mass of pulsars, and very good agreement between all four equations of state, and between both numerical codes, especially at low frequencies. The lowest braking index curves, occurring for pulsars with low baryonic masses, are not showing deviation from $n = 3$ at frequencies less than 160 Hz, which is highly inconsistent with observed braking index values.

In the model of isolated pulsars used in this work, the rate of change in rotational frequency of a spherical magnetized pulsar *in vacuo* depends on three factors: the MoI (constant or frequency dependent), the magnitude of the magnetic dipole moment, and the inclination angle between the magnetic and rotational axes. The braking index is related to the rate of change of these observables. We considered effects due to changes to the MoI and its variation, and showed that any significant deviation from the $n = 3$ value appears only at frequencies much higher than the frequency range of observed isolated pulsars with reliable braking index measurements. As MoI is related to the shape of the star, this result is consistent with the assumption of

the simple MDR model that the pulsar is spherical at low frequencies. We show in Figure 2.17 the correlation between the braking index and the deformation of the star in terms of the polar to equatorial radii ratio R_p/R_{eq} (normalized to 3 for display). It follows that changes in MoI alone cannot explain the observed deviation of the braking index at low frequencies from the simple MDR model predictions. If the MDR model is to be sustained, attention has to be paid to changes in the magnitude magnetic dipole moment and/or in the inclination angle. As stated above, the lack of knowledge of the origin and properties of the pulsar's magnetic field makes the former task difficult but the latter may be worth pursuing, particularly in view of the recent work by Lyne et al. (2013, 2015).

Finally, we have shown that the simple exclusion of the core due to superfluidity, or some superfluid barrier between the crust and core, does not have a strong effect on braking in the frequency range of observed isolated pulsars. Further development of the idea of a macroscopic description of superfluidity would be interesting. Changes to the magnetic field due to superfluidity and possible magnetic field expulsion, and a consequential increase in surface magnetic field strength B, could also be usefully explored. It is important to note that our simulation only accounts for the removal of core contribution to the rotation, and does not account for the rate of change of the mass contribution as a function of frequency due to the onset of superfluidity. Such considerations may also be important, even at low frequencies.

We conclude that the phenomenological investigation of superfluidity, simulated by eliminating the neutron star core from the total angular momentum of the pulsar, had a measurable effect at high frequencies. This may imply that superfluidity is a microscopic property inherent in the EoS, and has no significant influence on the moment of inertia of the star over long time periods. It should be noted, however, that we are only simulating a condition from some 'frozen in' superfluidity, and have not modeled dynamic superfluid differences in the interior of the star. Such a model may have a much larger impact on braking index as a function of time. This may be

implemented, for example, in the context of cooling over the characteristic age of the star.

Chapter 3

Low Frequency Dynamical MDR

The results from Chapter 2 show conclusively that changes in the moment of inertia as a function of frequency for a rotating pulsar, within the simple MDR model, cannot explain the braking indices obtained from measurement (Hamil et al., 2015). This is because the most reliable braking index data is limited to frequencies at or below around 30 Hz, where the moment of inertia of the star is essentially constant. Therefore, we include a possible constraint on the braking index model, at low frequencies, by allowing an increase in the angle of inclination between the magnetic moment and the axis of rotation.

Changes in the moment of inertia as a function of frequency, within the MDR model, do not explain the observed braking indices at frequencies below about 150 Hz. This is because the changes in shape, and thus the moment of inertia of the star, is negligible at low frequencies. In this chapter, we explore the MDR model with variable α, and present a parameter dependent set of solutions which would predict the braking index correctly if variation in α was observed. Inspired by the suggestion from Lyne *et al.* of possible observational evidence for a magnetic dipole migrating away from the rotation axis, we develop a toy model which shows that the magnetic field in the pulsar can be described, to first approximation, by two interacting dipoles, fixed to a finite length line between their centers, but allowed to rotate relative to one

another. Such a system generates enough magnetic energy to slow down the pulsar, by allowing α to increase with time.

The evolution of the angle of inclination between the rotational axis of the star and the dipole has been considered with interesting results. Lyne *et al.* investigated the effects of an increasing inclination angle on braking index (Lyne et al., 2015). It has been assumed that, over time, the magnetic moment should align itself with the axis of rotation, but there is some observational evidence for the angle to be migrating away from the rotational axis, although the authors stress that this idea is only one possible explanation of their observation (Lyne et al., 2015). Assuming this is the case, it provides a means by which the braking index can be affected at low frequencies. A rate of change in the inclination angle α will affect the $\sin^2 \alpha$ term in the MDR torque in Eq. 2.3, and results in a braking index that matches observation. Lyne *et al.*, used their predicted change in α from observation, $\dot{\alpha} = 0.6 \pm 0.03$ (degrees per century), and showed that this will reproduce the measured braking index value for the Crab pulsar if $\alpha = 45^0$.

So far, we have focused on finding the full dynamical range of the MDR model yielding a maximum physically meaningful deviation from the canonical value of the braking index, $n = 3$, as a function of rotational velocity. The effects of variation in the MoI of a rotating pulsar are only applicable to very fast rotating pulsars. For the low frequency region of the braking index curve, MoI in the MDR model is essentially constant, which leads to the canonical $n = 3$ for any object rotating at less than about 150 Hz.

We now investigate the consequence of variable α, and derive an expression for the energy loss by the rotating pulsar and its braking index under these conditions. We also develop a toy model of the pulsar magnetic field represented, to a first approximation, by two interacting dipoles. This model allows for α increasing with time, as measured from the axis of rotation, which results in recovery of the observed braking index values shown in Table 1.1 (Hamil and Stone, 2015).

3.1 The modification for changing alpha

As shown earlier, the energy loss by a rotating body with a constant MoI is proportional to a power of Ω. This relation leads to the power law $\dot{\Omega}$ = -K Ω^n where n is the braking index, equal to the ratio

$$n = \frac{\Omega\ddot{\Omega}}{\dot{\Omega}^2}. \tag{3.1}$$

Keeping with our investigation of the MDR model, we must revisit the dynamical derivation of the braking index. The derivation is the same as in Chapter 2, but now we consider the low-frequency side of the problem as defined in Section 1.2. We hold MoI constant, and allow for the physics of the braking mechanism to change with time (or frequency).

3.1.1 Dynamic extension of the MDR model revisited

As shown in Section 2.2.1, the expression for the braking index in the MDR model can be modified to include the dynamics of rotation. Taking the time variation of MoI and magnetic field into account will lead to a dynamical expression for n as a function of Ω in which we can choose to allow I, C, or both to evolve.

We start again with Eq. 2.10 from Section 2.2.1

$$\frac{d}{dt}\left(\frac{1}{2}I\Omega^2\right) = -C\Omega^4, \tag{3.2}$$

where $C = \frac{2}{3}R^6B^2sin^2\alpha$ contains the physics of the MDR braking mechanism. As detailed in Section 2.2.1, we derive a frequency dependent model of the braking index where either the MoI, or the physics contained in C change with frequency (or time). There is no reason MoI and the physics should not both change as a function of frequency, but as explained in Section 1.2, and shown in Chapter 2, we see that

the MoI dominates the braking index at high frequency, and the changing physics, whatever they may be, dominate at low frequency.

Continuing from the derivation in Section 2.2.1, we recall the resulting frequency dependent braking index model for MDR:

$$n(\Omega) \quad = \quad \frac{\Omega\ddot{\Omega}}{\dot{\Omega}^2} = 3 - \frac{(3\Omega I' + \Omega^2 I'')}{(2I + \Omega I')} + \frac{C'\Omega}{C}. \tag{3.3}$$

All eight reliable pulsars in Table 1.1 are rotating at frequencies near or below about 30 Hz, and have braking indices less than $n = 3$. At these frequencies, there must be an additional change in the physics to account for the measured braking index values. In the MDR model, the only physical parameters that can be changing at these frequencies are the surface field strength B, and angle of inclination between the magnetic dipole and the rotational axis of the pulsar. We leave out possible speculation of magnetic field expulsion, and other effects of changing field strength (Blanford and Romani, 1988; Contopoulos and Spitkovsky, 2006; Zhang and Xiee, 2012; Gourgouliatos and Cumming, 2014; Melatos, 1997), and instead focus on the evolution of the inclination angle, α in light of the recent work of Lyne et al. (2015, 2013).

Starting from Equation 3.3, we include $sin^2\alpha$ for the $\frac{C'}{C}$ term, while considering MoI and magnetic field strength to be constant. We find a dependence on α with frequency which leads to following equation;

$$n(\Omega) \quad = \quad 3 + 2\Omega \, \frac{\alpha'}{\tan\alpha}, \tag{3.4}$$

where the angle of inclination α is a function of frequency. For our initial investigation into changing inclination angle, it is more useful to consider α changing as a function of time as,

$$n(\alpha, \dot{\alpha}) \quad = \quad 3 + \frac{2\Omega}{\dot{\Omega}} \, \frac{\dot{\alpha}}{\tan\alpha} \tag{3.5}$$

The resulting calculation from Eq. 3.5 can be compared to the observational value for $\dot{\alpha}$ produced in Lyne et al. (2015, 2013).

It is worth mentioning the jerk parameter, m, at this point. The jerk parameter is similar to the braking index, but evokes the third derivative of rotational velocity, $\dddot{\Omega}$. In a few cases, the third derivative is known observationally. The jerk parameter can also be approximated using the braking index if the third derivative is not reliably known, but it should be noted that this adds no additional information to the braking index problem. The jerk parameter goes as follows:

$$m = \frac{\Omega^2 \dddot{\Omega}}{\dot{\Omega}^3}. \tag{3.6}$$

Similar to the treatment of n, we can derive a solution for m using our relations for Ω and its derivatives to get m as a function of $tan\alpha$, $\dot{\alpha}$, and also $\ddot{\alpha}$. The resulting equation becomes,

$$m(\alpha, \dot{\alpha}, \ddot{\alpha}) = 15 + \frac{9\Omega}{\dot{\Omega}} \frac{2\dot{\alpha}}{\tan\alpha} + \frac{\Omega^2}{\dot{\Omega}^2}\Big(\frac{2\dot{\alpha}}{\tan^2\alpha} - 2\dot{\alpha} - \frac{2\ddot{\alpha}}{\tan\alpha}\Big), \tag{3.7}$$

which could be used to further constrain the evolution of α, and set a more precise relation between α and its derivatives, if $\ddot{\alpha}$ can be found observationally. So far the third derivatives of rotational frequency are not well established, and the second derivative of α is not observationally apparent. Therefore, the jerk parameter is not important in the current work, but may become useful as pulsar observations improve.

3.2 Calculation with alpha

The effects of the time rate of change in α at low frequency (where MoI is constant) are investigated. In every case, the gravitational mass, radius, and magnetic field are calculated for a full range of allowed frequencies, starting from low frequencies which produce a static star, up to the limiting Kepler frequency where a star starts

to eject mass from its equator. In the case of changing α, all variables in the MDR mechanism except for the migration of the dipole moment are inconsequential in the current work. The obtained data is used in determination of the value of the braking index as a function of α, and $\dot{\alpha}$, as shown in Section 3.1.1.

We solve for the required change in the inclination angle α by using the braking index, and its measured values given in Table 1.1. In the MDR model, this allows the braking index to be matched to observed values at very low frequencies (below about 150 Hz) where I is approximately constant. This introduces the treatment as outlined in Section 3.1.1.

We obtain an analytical solution for $\dot{\alpha}$ by using the known values of Ω, $\dot{\Omega}$, and the braking index with the only free parameter being $\tan\alpha$. The $\tan\alpha$ parameter is set by the results reported by Lyne *et al.*, where they found it to be $\tan\alpha = 1$, or $\alpha = 45^0$. With this assumption, it is easy to solve for the remaining pulsars with well known braking indices in order to find $\dot{\alpha}$ if the conditions were found to be similar to those observed in the Crab pulsar.

Additionally, it is useful to investigate the relationship between $\dot{\alpha}$ and $\tan\alpha$ for arbitrary angles between zero and ninety degrees. For each fixed value of n, Ω, and $\dot{\Omega}$, we plot the solution to $\dot{\alpha}$, and α, in order to set a parameter that may be used if any of these values should be seen observationally.

3.3 Changing alpha results

In light of possible observational evidence for the angle α to be migrating away from the axis of rotation, we show that it provides a means by which the braking index can be matched with observation at low frequencies. We employ the braking index, and known values of Ω and $\dot{\Omega}$, to solve for $\dot{\alpha}$ analytically while assuming conditions similar to those found in the Crab pulsar by Lyne *et al.*. We are able to reproduce the results of Lyne *et al.* for the Crab pulsar, and obtain results for the remaining pulsars.

Table 3.1: Calculated values of $\dot{\alpha}$ based on the braking index, with the assumed condition imposed from Lyne *et al.*that $\tan\alpha = 1$.

Pulsar	n	α (Degrees)	$\dot{\alpha}$ $\left(\frac{deg}{100yrs}\right)$
PSR B0531+21 (Crab)	2.51±0.01	45	0.56 ± 0.012
PSR B0540−69	2.140±0.009	45	0.739 ± 0.0075
PSR B0833−45 (Vela)	1.4±0.2	45	0.203 ± 0.026
PSR B1509−58	2.837	45	0.15 ± 0.00
PSR J1846−0258	2.16±0.13	45	1.65 ± 0.26
J1833−1034	1.8569±0.0006	45	0.3371 ± .0002
PSR J1119−6127	2.684	45	0.281 ± 0.00
PSR J1734−3333	0.9±0.2	45	0.259 ± 0.025

It can be seen that an analytical solution for $\dot{\alpha}$ can be obtained by using the known values of Ω, $\dot{\Omega}$, and the braking index with the only free parameter being $\tan\alpha$. If $\tan\alpha$ is set to $\tan\alpha = 1$, or $\alpha = 45^0$, as reported by Lyne *et al.* for the Crab pulsar, then it is straight forward to solve for the remaining pulsars from Table 1.1, to find $\dot{\alpha}$ solutions. The results are presented in Table 3.1 showing reasonable rates of change in α for all pulsars.

In addition to the above analytical approach, we have employed a numerical solution to the relation between α and $\dot{\alpha}$ for arbitrary values of α ranging from approximately zero to ninety degrees. The resulting curves are given in the upper part of Figure 3.1. Each curve represents the relation between $\dot{\alpha}$ and α over the range of allowed angles, for the individually known values of n, Ω, and $\dot{\Omega}$ pertaining to each pulsar as given in Table 1.1. The lower part of Figure 3.1 shows the braking index as a function of $\dot{\alpha}/\tan\alpha$ for the fixed ratio of $\Omega/\dot{\Omega}$ pertaining to each individual pulsar. The curves can be used for determination of α provided the braking index and $\dot{\alpha}$ would be known simultaneously from observation.

We see from Figure 3.1 that as the dipole moment approaches orthogonality, the braking index asymptotically approaches zero. This shows that the pulsar may be eventually killed by increasing α, but a realistic time calculation of this process is necessary to make such a prediction. The time rate of change of the angle is very

slow, and only known for the length of our current observation. Therefore we cannot predict, with any certainty, a correlation between increasing α and the pulsar death line.

3.4 Toy model of two interacting dipoles

The origin and distribution of the *assumed* magnetic field of a pulsar, and its misalignment with respect to the axis of rotation are not well understood. There is extensive literature on this subject, documenting the complexity of the problem (see e.g. Spruit (2008); Fujisawa and Kisaka (2014); Potekhin (2014)).

There is very little observational evidence for the existence and intensity of pulsar magnetic fields. The only "direct" evidence comes in the form of radiation from pulsars accreting material from a binary partner (Coburn et al., 2003) which has been associated with cyclotron resonance of electrons orbiting the field lines. The resonance frequencies correspond to fields of up to (1−4) x 10^{12} Gauss (Reisenegger, 2003). In isolated pulsars, the field is usually derived from the relation between the period of rotation and spin down, assuming MDR, using the formalism detailed in Hamil et al. (2015) and this work. The values obtained are of the order of 10^{12} Gauss. Existence of objects with extremely strong surface magnetic fields, up to 10^{15-16} Gauss, based on observation of high energy X-ray and gamma-rays (magnetars) seem to be generally accepted (Harding and Lai, 2006).

The two principal sources of magnetic field in pulsars most frequently discussed are the dynamo effect and constituents magnetization. The dynamo theory describes the process by which a rotating, convecting, and electrically conducting fluid acts to maintain a magnetic field. It requires kinetic energy, which is provided by the pulsar rotation, and an internal energy source to drive convective motions within the fluid (Thompson and Duncan, 1993). Existence of a stable ferromagnetic core inside the liquid interior of the pulsar has been discussed by many authors in the past (see e.g. Haensel and Bonazzola (1996) and ref. therein) and has been recently

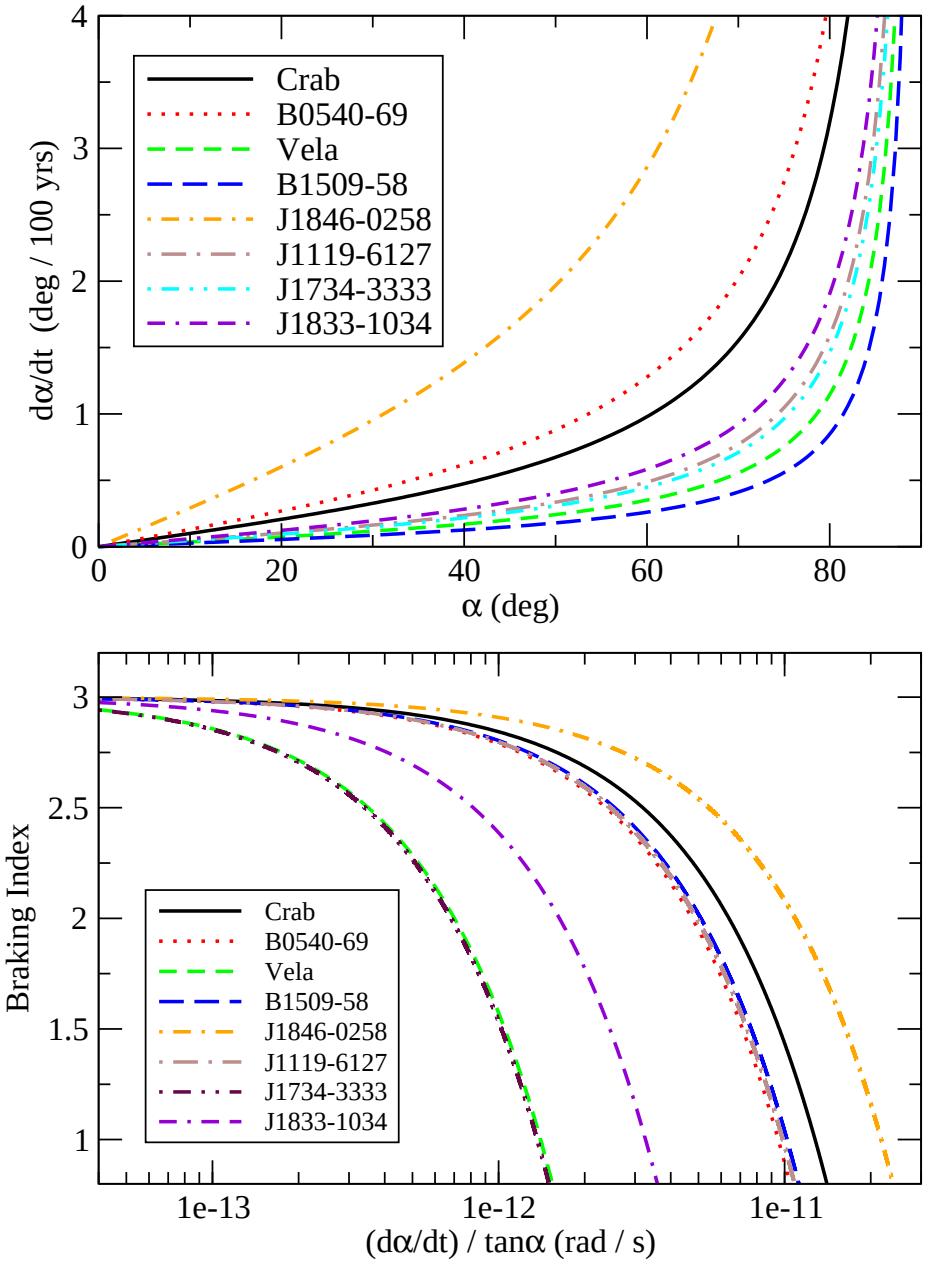

Figure 3.1: (Color on-line) Solution of the required rate of change of the inclination angle between magnetic moment and axis of rotation, for arbitrary angle between zero and 90 degrees, assuming constant braking index. The eight reliable pulsars are shown. The second plot shows the value of braking index as a function of the ration of $\dot{\alpha}/\tan\alpha$.

revived (Eto et al., 2013; Hashimoto, 2015). The ferromagnetic material may have a domain structure which would lead to a magnetic field that is not con-centric with the rotational axis.

Although the magnetic field inside pulsars is likely a complicated configuration, it is assumed, to first approximation, to be dominated by a dipolar term. The dipole explains the observed pulse, and the estimated power radiated due to rotation; however, there is no intrinsic reason to discount possible additional magnetic fields that go unseen because they are overwhelmed by the first order observed dipole radiation. In this work we will consider two dipoles existing within the star. The first comes from the dynamo effect, and is centered in the star, pinned to the axis of rotation. The second is a stronger dipole that is the resultant of ferromagnetic material in the star.

As stated above, the magnetic field in this work will manifest in two different ways: either by charged particles travelling in a current (dynamo effect), or in the alignment of many particles, each with dipole moments (ferromagnetism). Both of these originating conditions can surely exist within neutron stars, and therefore it is not altogether unreasonable to assume they may co-exist. In this case the dipole moments of the two configurations may interact in a way that causes one, or both, of them to migrate toward orthogonality with respect to the axis of rotation. Here we present a toy model of interacting dipoles which makes a crude first order attempt to define the possible physics behind the increase in α seen by Lyne *et al.*, which can account for the braking index of the Crab pulsar.

3.4.1 Potential energy configuration

If we assume that there are two dipoles existing in the neutron star, separated by some distance r that is held radially fixed at some angle with respect to the axis of rotation, the potential energy for their interaction can be calculated. We can conceive of a few configurations which will seek lower energy, and thus one or both of

the dipoles can rotate, resulting in a lower energy state configuration. We will first outline the derivation of the energy, and give examples of solutions. Later, we will speculate as to the different possible configurations and comment on the remaining physical assumptions required.

In this model, we will define two dipoles, $\vec{m_1}$ and $\vec{m_2}$, which are fixed along a line, $\hat{r}$, connecting their centers, and oriented with angles θ_1 and θ_2, respectively, to $\hat{r}$ as illustrated in Figure 3.2. The first dipole, $\vec{m_1}$, represents the dynamo effect, and is pinned to the center of the star with fixed angle, θ_1. The second dipole, $\vec{m_2}$, is the resultant of the sum of dipole moments in the ferromagnetic material in the star which is held at fixed distance r, but allowed to rotate through angle θ_2. The motion of $\vec{m_2}$ is also illustrated in Figure 3.2. Next, we will derive an expression for the potential energy of our two dipole interaction.

Starting with the magnetic field of dipole $\vec{m_1}$,

$$\vec{B_1} = \frac{\mu_0}{4\pi}\frac{1}{r^3}[3(\vec{m_1}\cdot\hat{r})\hat{r} - \vec{m_1}], \tag{3.8}$$

where μ_0 is the magnetic permeability of free space, $\vec{m}$ is the magnetic moment of the dipole, and $\hat{r}$ is the line from the center of the dipole extending a distance r. The potential energy of the magnetic dipole with moment, $\vec{m_2}$ in the magnetic field of the first dipole with magnetic field, $\vec{B_1}$ is given as

$$U_{12} = -\vec{m_2}\cdot\vec{B_1}, \tag{3.9}$$

the energy of the interaction between two dipoles reads as

$$U = \frac{\mu_0}{4\pi}\frac{1}{r^3}[3(\vec{m_1}\cdot\hat{r})(\vec{m_2}\cdot\hat{r}) - \vec{m_1}\cdot\vec{m_2}]. \tag{3.10}$$

Now we assume that two dipoles are fixed along a line bisecting both so that each dipole moment makes an angle θ_1 and θ_2, with respect to the line. In this case, the

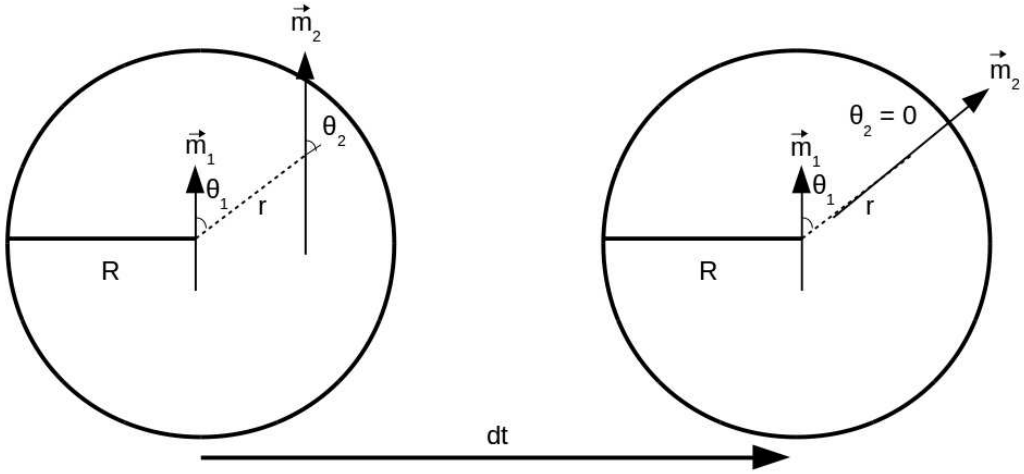

Figure 3.2: (Color on-line) Example of possible configuration of the magnetic field interaction inside a neutron star modeled as two simple dipoles. The central dipole $\vec{m_1}$ is held fixed to the center of the star, and $\vec{m_2}$ is offset at a fixed distance defined by r. The centered dipole is held fixed with angle θ_1 with respect to $\hat{r}$, while the offset dipole $\vec{m_2}$ is allowed to arbitrarily rotate through angle θ_2, also with respect to $\hat{r}$. This configuration is exaggerated for illustration, but in the case of the Crab pulsar, we will assume that the initial and final values for θ_2 are very close to zero (as measured over 100 years by Lyne *et al.*)

interaction energy can be worked out as a function of both angles. The energy of the configuration becomes,

$$U = \frac{\mu_0 m_1 m_2}{4\pi r^3}(\sin\theta_1 \sin\theta_2 - 2\cos\theta_1 \cos\theta_2). \tag{3.11}$$

Assuming the interacting dipoles are in some initial configuration, they will progress over time toward a final configuration as long as the interaction energy has reduced. There are a few scenarios that we can consider, and it turns out that as long as the energy allows the scenario, the initial and final configurations of the moments does not have a large effect on the result. We can start both dipoles parallel to the axis of rotation, and then let them both migrate toward $\theta_1 = \theta_2 = 0$, or we can hold one fixed to the axis of rotation while the other is allowed to rotate freely, etc. Because of the very large magnetic fields associated with pulsars, the change in energy coming from these different configurations is not significant compared to the product of the magnitude of magnetic moments m_1 and m_2 in Eq. 3.11.

The illustration in Figure 3.2 represents the initial and final configuration that we will explore in this work. The initial configuration has magnetic moment $\vec{m_1}$ pinned to the center of the star, and $\vec{m_2}$ is allowed to rotate at a fixed distance r from $\vec{m_1}$. Both moments are initially parallel to the axis of rotation and angles θ_1 and θ_2 with respect to $\hat{r}$. After some time, $\vec{m_2}$ rotates until its angle θ_2 has reduced to zero. We assume, in this model, that $\vec{m_2}$ represents the measured dipole moment in the neutron star. In this case, α is the angle between $\vec{m_2}$ and the (vertical) axis of rotation. This way, as θ_2 approaches zero, α approaches the initial angle we chose for $\hat{r}$ with respect to vertical. Thus we can set the final angle of α by our choice of $\hat{r}$. In this study, we will set $\hat{r}$ at 45^0 in keeping with the results of Lyne *et al.*.

We now can relate the potential energy of the dipole to the kinetic energy of its motion. We initially assume that the angle we measure is θ_2 in our configuration. We must assume here that the measured dipole, $\vec{m_2}$, is pinned to some portion of the material in the star as it rotates. This way, we can estimate the moment of inertia

as some fraction of the pulsar's total MoI. This is done, in general, by assuming that the dipoles are similar enough in motion that they may be approximated by only one angle, or that one dipole is fixed, so it only facilitates the motion of the other, and we only have one changing θ. In our model, we consider only the second option, so θ_2 is moving while θ_1 is fixed to the rotational axis of the pulsar. Since $\vec{m_1}$ is fixed to the center of the star, the total kinetic energy involves only the rotating dipole, $\vec{m_2}$. In the following derivation of the motion of θ_2 we note that as θ_2 *decreases* toward $\hat{r}$, so too α *increases* away from the vertical axis of rotation. It is clear that $\dot{\theta}_2 = -\dot{\alpha}$. So we continue with our calculation of $\dot{\theta}_2$ below, but understand that the values obtained will be equivalent in magnitude to the possible $\dot{\alpha}$ described in Section 3.3. See section 3.5 for discussion of other possible configurations.

Assuming we are measuring the motion in the limit of one rotating dipole carrying some portion of the total moment of inertia of the pulsar, we have only one kinetic energy term. In the following, we consider θ_1 to be fixed to the center of the star, and θ_2 is allowed to rotate which results in an expression for $\dot{\theta}_2$,

$$\frac{1}{2} I \dot{\theta}_2^2 = \Delta U = U_f - U_i, \tag{3.12}$$

where U_f and U_i are the final and initial configurations of the dipole moments respectively. Eq. 3.12 becomes,

$$\frac{1}{2} I \dot{\theta}_2^2 = \frac{\mu_0 m_1 m_2}{4\pi r^3} F \tag{3.13}$$

where,

$$F = (\sin\theta_{1f} \sin\theta_{2f} - 2\cos\theta_{1f}\cos\theta_{2f}) - (\sin\theta_{1i}\sin\theta_{2i} - 2\cos\theta_{1i}\cos\theta_{2i}) \tag{3.14}$$

is a simple function that we define here for ease of calculation.

Solving for our rotation rate we have an equation for $\dot{\theta}$,

$$\dot{\theta}_2^2 = \frac{2\mu_0 m_1 m_2}{4\pi I r^3} F \tag{3.15}$$

where m_1 and m_2 are the magnitudes of the dipole moments, I is the moment of inertia of the rotating portion of the star, and r is the distance between the centers of the dipoles.

It is convenient to express Eq.3.15 in cgs units:

$$\dot{\theta}_2^2 = \frac{2 m_1 m_2}{I r^3} F. \tag{3.16}$$

3.4.2 Calculation of $\dot{\theta}_2$

The calculation of Eq. 3.14 can be done in a very straight forward way. We initially seek any solution which results in a lower energy for the final configuration. These negative solutions, depending on the initial and final values taken for θ_1 and θ_2, range in value from a high value of three and approach the limit of zero if we assume very little change in the configuration. In light of the Lyne observations, we make certain assumptions. Firstly, the Lyne observation of the Crab pulse gives the angle at roughly 45^0, so we will set the line connecting the two dipoles, $\hat{r}$, at 45^0 with respect to the equator of the star, so both initial angles for each dipole is at 45^0 with respect to $\hat{r}$ (see Figure 3.2). Secondly, we adopt the configuration where one dipole is pinned to the center of the star, while the second is allowed to rotate carrying some fraction of the MoI of the star. If θ_2 goes to zero, it has moved 45^0 and sets the value of $F = 0.91$. In order to test the Lyne result, however, we require the observed value for $\dot{\alpha}$, which sets a total motion of α over 100 yrs which is much smaller than 45^0. Using the results of Lyne *et al.* we will assume that the $\alpha = 0.785$ radians, and $\dot{\alpha} = 3.32 \times 10^{-12}$ radians/s. This requires that θ_1 is set at 45^0 with respect to $\hat{r}$, but θ_2 is initially set to a smaller value corresponding to its motion over 100 yrs as

measured by Lyne. Using these values, we can obtain the amount of change in α, and θ_2 by extension.

With these considerations, the central dipole is pinned, the line connecting the two dipoles is at 45^0 with respect to the axis of rotation, and the second dipole has moved roughly 0.01 *radians* over 100 years (note: 100 yrs is the time frame used by Lyne to calculate $\dot{\alpha}$). These conditions, valid only for the Crab pulsar, result in the value of $F = 0.00672$.

We are now in a position to investigate the parameters required for the dipole interaction. We start with Eq. 3.16, and rearrange for our known values such that,

$$\frac{m_1}{r^3} = \frac{I\dot{\theta}_2^2}{2m_2F} \tag{3.17}$$

where m_2 is the dipole moment magnitude of the measured pulse, m_1 is the central dipole magnitude, and r is the distance between the dipole centers. We require that the value of $\dot{\theta}_2$ has the same magnitude as $\dot{\alpha}$, and that I is on the order of some fraction of the MoI of the star. We can go one step further by noting that r is some fraction of the radius R of the pulsar;

$$m_1 = \left(\frac{r}{R}\right)^3 \frac{I\dot{\theta}_2^2}{2BF} \tag{3.18}$$

where $(r/R)^3$ is the ratio of the distance between dipoles to the radius of the star, and B is the magnetic field of the pulsar as calculated in the $P\dot{P}$ diagram.

We are free to choose the values of r, the initial and final angle associated with the rotating dipole moment, θ_2, and the time over which the rotation occurs. We have chosen reasonable values for these, and included the results in Table 3.2. For the values calculated, we choose the ending position for the measured dipole moment to be 45^0 from the axis of rotation, the value of $m_2 = 10^{30}$ erg/G (from the canonical $B = 10^{12}$ G and $R = 10^6$ cm), and expect that the time is on the order of the

Table 3.2: Calculated values of the central dipole moment, m_1 with respect to the allowed change in angle θ_2 ($\dot{\alpha}$), and the distance of moment m_2 from the center of the star. The units are as follows: $r[10^6\text{cm}]$, $\Delta\alpha$ [degrees/100yrs], $\dot{\alpha}[10^{-12}\text{radians/s}]$, and m_1 [erg/G].

	$\Delta\alpha = 0.6^0$ $\dot{\alpha} = 3.32$	$\Delta\alpha = 1.0^0$ $\dot{\alpha} = 5.53$	$\Delta\alpha = 10.0^0$ $\dot{\alpha} = 55.3$	$\Delta\alpha = 25.0^0$ $\dot{\alpha} = 138$	$\Delta\alpha = 45.0^0$ $\dot{\alpha} = 249$
$r = .0001$	0.7369	1.220	10.62	22.19	33.92
$r = .001$	736.9	1.220×10^3	1.062×10^4	2.219×10^4	3.392×10^4
$r = .01$	7.369×10^5	1.220×10^6	1.062×10^7	2.219×10^7	3.392×10^7
$r = .1$	7.369×10^8	1.220×10^9	1.062×10^{10}	2.219×10^{10}	3.392×10^{10}
$r = .2$	5.895×10^9	9.758×10^9	8.492×10^{10}	1.775×10^{11}	2.714×10^{11}
$r = .4$	4.716×10^{10}	7.806×10^{10}	6.794×10^{11}	1.420×10^{12}	2.171×10^{12}
$r = .6$	1.591×10^{11}	2.635×10^{11}	2.293×10^{12}	4.793×10^{12}	7.327×10^{12}
$r = .8$	3.773×10^{11}	6.245×10^{11}	5.435×10^{12}	1.136×10^{13}	1.737×10^{13}
$r = .9999$	7.369×10^{11}	1.220×10^{12}	1.062×10^{13}	2.219×10^{13}	3.392×10^{13}

history of pulsar observations, all of which are consistent with the results of Lyne et al. (2015).

Using the known values for the Crab pulsar in Eq. 3.18, and defining the distance between the dipole centers on the order of 1 km, we get a value for the centered dipole moment of about $m_1 = 7.37 \times 10^8$ erg/G. This represents a very small magnetic dipole pinned to the center of the star. Depending on the physical parameters of this dipole, it may have a very small magnetic field which would be undetectable at the surface of the star compared to the measured dipole field. This calculation can be made for the remaining pulsars in the data, but the result for the Crab is illustrative of one possible mechanism for changing α.

From the results shown in Table 3.1, we calculate values of m_1 for all eight pulsars. The results shown in Tables 3.3 and 3.4 are similar to those in Table 3.2, but are calculated based on the change in angle found in Table 3.1. We have chosen a value of r that represents a position anywhere within the radius of the star starting from 1 meter all the way to the edge of the star. It is assumed that the resultant dipole representing the sum of magnetic moments may be arbitrarily centered somewhere between the center of the star and the crust. We include the asymptotic limit of

Table 3.3: Part 1: Calculated values of the central dipole moment, m_1 with respect to the allowed change in angle θ_2, and the distance of moment m_2 from the center of the star, using the calculated values shown in Table 3.1. The units are as follows: $r[10^6\text{cm}]$, $\Delta\alpha$ [degrees/100yrs], $\dot{\alpha}[10^{-12}\text{radians/s}]$, and m_1 [erg/G].

	PSR B0531+21	PSR B0540-69	PSR B0833-45	PSR B1509-58
	$\Delta\alpha = 0.56^0$ $\dot{\alpha} = 3.10$	$\Delta\alpha = 0.74^0$ $\dot{\alpha} = 4.09$	$\Delta\alpha = 0.20^0$ $\dot{\alpha} = 1.11$	$\Delta\alpha = 0.15^0$ $\dot{\alpha} = 0.831$
$r = .0001$	6.882×10^{-1}	9.054×10^{-1}	2.473×10^{-1}	1.857×10^{-1}
$r = .001$	6.882×10^{2}	9.054×10^{2}	2.473×10^{2}	1.857×10^{2}
$r = .01$	6.882×10^{5}	9.054×10^{5}	2.473×10^{5}	1.857×10^{5}
$r = .1$	6.882×10^{8}	9.054×10^{8}	2.473×10^{8}	1.857×10^{8}
$r = .2$	5.506×10^{9}	7.243×10^{9}	1.979×10^{9}	1.485×10^{9}
$r = .4$	4.405×10^{10}	5.795×10^{10}	1.583×10^{10}	1.188×10^{10}
$r = .6$	1.487×10^{11}	1.956×10^{11}	5.342×10^{10}	4.010×10^{10}
$r = .8$	3.524×10^{11}	4.636×10^{11}	1.266×10^{11}	9.506×10^{10}
$r = .999\bar{9}$	6.882×10^{11}	9.054×10^{11}	2.473×10^{11}	1.857×10^{11}

$r = 0.999\bar{9}$ for completeness, but realize it is unlikely that a dipole is centered at the surface of the pulsar. We have shown that, for the results expected in agreement with the results of Lyne *et al.*, the value of the centered dipole m_1, is sufficient to cause the required rotation, but small enough to go undetected, and is positioned reasonably inside the radius of the pulsar.

3.5 Discussion

The result shown for the Crab pulsar is for one configuration where every effort was made to find a realistic scenario. Given the value for $\dot{\alpha}$, and the assumed parameters for the Crab (i.e. $B = 10^{12}$ G, etc.), the result is essentially an upper limit to the value of the centered dipole moment. This effort is made because it may be difficult to make the case that a very small centered dipole will have the required effect. There are additional considerations that must be accounted for, such as conservation of angular momentum (which leads to a precession of the dipole moment and may be in the direction of its rotation), that are not accounted for in this work.

Table 3.4: Part 2: Calculated values of the central dipole moment, m_1 with respect to the allowed change in angle θ_2, and the distance of moment m_2 from the center of the star, using the calculated values shown in Table 3.1. The units are as follows: $r[10^6\text{cm}]$, $\Delta\alpha$ [degrees/100yrs], $\dot{\alpha}[10^{-12}\text{radians/s}]$, and m_1 [erg/G].

	PSR J1846-0258	PSR J1833-1034	PSR J1119-6127	PSR J1734-3333
	$\Delta\alpha = 1.65^0$ $\dot{\alpha} = 9.13$	$\Delta\alpha = 0.34^0$ $\dot{\alpha} = 1.88$	$\Delta\alpha = 0.28^0$ $\dot{\alpha} = 1.55$	$\Delta\alpha = 0.26^0$ $\dot{\alpha} = 1.44$
$r = .0001$	1.991×10^{1}	4.194×10^{-1}	3.458×10^{-1}	3.212×10^{-1}
$r = .001$	1.991×10^{3}	4.194×10^{2}	3.458×10^{2}	3.212×10^{2}
$r = .01$	1.991×10^{6}	4.194×10^{5}	3.458×10^{5}	3.212×10^{5}
$r = .1$	1.991×10^{9}	4.194×10^{8}	3.458×10^{8}	3.212×10^{8}
$r = .2$	1.592×10^{10}	3.355×10^{9}	2.766×10^{9}	2.569×10^{9}
$r = .4$	1.274×10^{11}	2.684×10^{10}	2.213×10^{10}	2.056×10^{10}
$r = .6$	4.299×10^{11}	9.060×10^{10}	7.469×10^{10}	6.938×10^{10}
$r = .8$	1.019×10^{12}	2.148×10^{11}	1.770×10^{11}	1.645×10^{11}
$r = .9999$	1.991×10^{12}	4.194×10^{11}	3.458×10^{11}	3.212×10^{11}

The interpretation of this particular model is that there is a small dipole field at the center of the pulsar which is pinned to the axis of rotation. This is possibly because the dipole is a result of charged fluid rotating in-line with the star. It may be very small and only generated in the inner core of the star. The second field may be the sum of all the moments of the ferromagnetic material in the star. The second field, as far as 100 years ago, is misaligned with rotation almost to 45^0, and has migrated very slowly due to interaction with the centered dipole.

The MoI may be thought of as the sum of all of the "chunks" of magnetic material (or particles) as they very slowly rotate due to the fixed dipolar field resulting from the central dynamo. It is important to note here that any material in the star which contributes to the ferromagnetic dipole moment is also subject to rotational forces. Coriolis, and centrifugal effects may be important, but are neglected in this work to a first approximation.

We note that the interpretation can possibly be different. For example, the weaker field could be frozen into the crust of the star, and the stronger field is pinned in the superfluid material which may rotate inside the star. The secondary field may

also come from particles in the magnetosphere which are simply not connected to the rotation of the star. We assume the scenario described in this thesis, but acknowledge there may be multiple explanations. We maintain that ferromagnetic moments in a dynamo induced, centered, dipole field is the most promising description for our toy model.

3.6 Summary and outlook

In light of recent evidence that the angle of inclination between the magnetic moment and axis of rotation is migrating toward the equator of the star, we have investigated how this change might affect the braking index. More specifically, we have investigated how this change must manifest at low frequencies in order to recover known observational values for the braking index. We know that the observed braking indices for which the data is reliable exist only for pulsars whose frequencies are well below the threshold beyond which rotational effects have any significant impact. Because of this, we also know there must be a mechanism by which the braking index can change in the range of frequency where rotational effects are negligible. The only possibility in the MDR model for such a mechanism is a change in the magnetic moment. In this case, it is quite interesting that there is observational evidence of such a change.

We investigated the changing angle α in two ways. We first assumed, for each pulsar, that conditions shown by Lyne *et al.* for the Crab are realized. In this way, we have a value for α as it exists today, along with the known frequency and braking index, for which we can solve for $\dot{\alpha}$. In so doing, we have created a table of values which one may expect to see for each pulsar, assuming that the conditions found by Lyne *et al.* for the Crab pulsar are consistent.

Secondly, we can assume that the conditions vary between pulsars, and as such, the value attained by Lyne for the α of the Crab pulsar is not known in any of the remaining pulsars in our study. In this case, we have a two variable system with only

one equation. In order to provide some insight into the possible evolution of α in each of the pulsars, we allow α to run from approximately zero up to ninety degrees, and solved for the corresponding values of $\dot{\alpha}$. This results in a plot representing the relation between α and $\dot{\alpha}$ for the pulsars in Table 1.1. Figure 3.1 gives a range of values which may be expected to be seen upon further analysis of data similar to that studied in Lyne et al. (2015). For a given α or $\dot{\alpha}$, one may be able to match data in our curves. This also gives insight into the behavior of pulsars as α migrates outward. It can be seen from Figure 3.1 that as the angle increases, the rate of change increases as $\tan\alpha$. This suggests that the evolution of α causes a significant impact on rotation that blows up as α approaches 90^0. It can be speculated that an angle above the 80^0 range may effectively kill the pulsar, although much more investigation is required to substantiate such a claim.

Finally, we have constructed a toy model of one possible mechanism which may cause α to migrate. We assume some complicated magnetic field interaction which may be approximated by two simple interacting dipoles. For example, this situation could occur if the large measured dipole was the resultant of the sum of the magnetic dipoles of ferromagnetic material in the star (Hashimoto, 2015), slightly offset from the center of the star, which interacts with a smaller dipole, located at the center of the star, resulting from a rotating conducting fluid. This configuration results in a potential energy configuration that will seek a lower energy state over time. If only the measured dipole moment is allowed to rotate while its center is held at some finite distance from the center of the secondary dipole as shown in Figure 3.2, the value for $\dot{\alpha}$ required to solve the braking index obtained in Lyne et al. (2015) (at least for the Crab) is recovered. This interaction is a very simple first order approximation, but it has the advantage of solving the problem with a plausible configuration. It should be noted that this toy model may be expanded with considerations of conservation of angular momentum, precession of the offset dipole as it rotates, and rotational forces acting within the star. This model may also be improved with increased knowledge of the nature and origin of the pulsar magnetic field in general.

Chapter 4

Conclusions and future goals

In this research, our aim was to identify and investigate the well known problem of the divergence of the observed spin evolution of pulsars, with the theoretical predictions. We have assumed that pulsars are neutron stars which carry a detailed set of parameters that are useful in the multifaceted study of many different aspects of physics. In this work, we have studied a combination of astrophysics, nuclear-particle physics, the physics of complex magnetic fields, general relativity, and the parameterization of ultra-dense cold matter through investigation of the spin evolution of pulsars. We explored a wide range inquiry into the dynamical possibilities of the braking index in the framework of magnetic dipole radiation (MDR).

In rotationally powered, isolated pulsars, the predominant mechanism of the observed spin down is attributed to MDR. If the star can be considered to be a large magnetic dipole that is misaligned to the axis of rotation of the star, it will radiate electro-magnetic energy into space. This description fits the observed phenomena of pulsars well, and explains why they shine like lighthouses in the sky. It is well known, however, that this MDR description of pulsars leads to a definite value for the braking index, $n = 3$, which is not found in nature. The aim of this research was to find a reasonable solution to this issue by examining the MDR braking index model from

a dynamical description based on neutron star properties generated from physically realistic equations of state (EoS).

We re-derived the braking index model, in the framework of MDR, to allow for physical parameters in the physics of the pulsar to change with frequency (or time). This exercise leads to the realization that the dynamic braking index is dominated at high and low frequencies by different aspects of the model. It also provides, for the first time, the inclusion of physical properties of neutron stars to the model. Because of this unique aspect of the work, we were able to introduce physically realistic EoS, and model the braking index over a range of baryonic masses, at all available frequencies.

Our preliminary investigation shows how the braking index changes if the moment of inertia (MoI) of the star is increased as a function of frequency while the physics in the MDR torque (magnetic moment strength, and inclination angle) are held constant. We modeled neutron stars based on four physically realistic EoS over a range of baryonic mass of $1.0M_{\odot} < M_{\rm B} < 2.2M_{\odot}$ with frequencies ranging from zero to the Kepler (mass shedding) frequency of each star. We employed state of the art computational methods to generate the neutron star macro-properties by using two sophisticated rotating neutron star codes (Negreiros, 2012; Weber, 1999, 2013). Our investigation yields the full allowed range of braking index as a function of frequency with constant magnetic field. While our results recover the measured braking index values, they do so at frequencies that are much higher than those of the measured pulsars with reliable braking indices shown in Table 1.1. We have shown conclusively that the effects of changing moment of inertia alone cannot affect the braking index values of pulsars that are rotating at anything less than about 150 Hz. For pulsars in this range, we need to approach the problem in the low-frequency range.

Because all of the reliable braking index observations (see Table 1.1) come from pulsars rotating at approximately 30 Hz or less, the changing MoI cannot have any measurable effect. This leads to the low frequency portion of the research where we allow the variable physics in the MDR mechanism to evolve in time. This amounts to allowing the magnetic dipole moment to change. There are two ways this can

manifest. Either the surface strength of the magnetic field increases as the pulsar spins down, or the angle of inclination α of the magnetic moment to the axis of rotation of the star increases over time. The first option, while plausible, is merely a source of speculation at this point (Blanford and Romani, 1988) since the origin and configuration of the pulsar magnetic field is not well understood. The evolution of the angle of inclination is interesting in light of the recent paper by Lyne et al. (2015), because they find reasonable evidence of the required change in α that solves the braking index for the Crab pulsar. Continuing with the result of Lyne *et al.*, we calculate the results for the remaining pulsars described in Table 1.1 analytically. In addition, we calculate a numerical parameterization of the allowed changes in α as a function of braking index with no assumed knowledge of the Lyne results for the Crab. This provides a template from which to verify braking indices in the event that future observations of α migration, in general, become available.

Aiming to describe a first order approximation of one possible description of the physics that would produce the results of Lyne *et al.*, we formulated a toy model that can produce the measured change in α. We assume that there may exist some complicated magnetic field within the pulsar that may be approximated by two interacting magnetic dipoles. This could manifest, for example, if there was a dipole centered with the axis of rotation of the star due to a rotating conductive fluid, and then a second dipole which is the resultant of the assembly of magnetic moments of ferromagnetic material in the star (Hashimoto, 2015). In this simple model, the two interacting dipoles have an initial potential energy between them, and seek a lower energy state at some later time. We find that this is possible if one, or both, dipoles are allowed to rotate while fixed at some finite radial distance to each other. Our result shows that the measurements of Lyne *et al.* are reproduced if there is a relatively small dipole pinned to the center of the star, and the secondary (observed) dipole is allowed to rotate even very slightly.

To summarize, we investigated the dynamic treatment of the MDR braking index for all possible frequencies. We used neutron star macro-properties, developed from

physically realistic equations of state, modeled with state of the art computational methods, in order to calculate the braking index as a function of frequency. We managed to recover known braking index values at both high and low frequency considerations. It is interesting, however, that all reliable braking index observations occur in the low frequency range where changes in moment of inertia are irrelevant because this requires changes in the magnetic field to provide a valid solution. Following the worked of Lyne *et al.* such a solution can be realized. It is also notable that there are only eight reliable braking index measurements out of hundreds of observed pulsars. Many pulsars have very high frequencies which may imply some importance to the changing MoI in their braking indices which are not reliably known as of yet. Perhaps, in the near future, as more observations become available, braking indices of high frequency pulsars may be studied in the context of changing MoI.

4.1 Future study

In the future, we would like to model the braking index over the full range of frequencies considering all possible mechanisms. We have a very good handle on the physics of MDR over the two regions, but to bridge the gap, we need to learn more about rotationally driven effects on neutron star magnetic fields and composition. It will be worthwhile to apply the current work on magnetic moment to the relativistic wind braking index mechanism, and to couple this to the MDR by the polynomial shown in Carraminana and Alvarez (2004). The addition of realistic neutron star properties, and the effects of rotation should improve the polynomial model. This work has not been done in the context of rotation, and we now have models in place that will enhance the investigation. A combination of MDR and pulsar wind, along with magnetic field evolution and changing MoI is worthy of further investigation, and this should be done as soon as possible.

Additionally, it would be very useful to explore the full magnetohydrodynamics of neutron stars, and formulate some mechanism that will actually increase surface

magnetic field strength as a function of frequency (or time). Magnetic field line expulsion due to superfluidity is one consideration that manifests itself in cooling models, but has not been used in braking index research specifically. There may be other factors at work, in the magnetosphere for example, that increase magnetic field with spin-down. The toy model defined in Section 3.4 is also dependent on a correct description of the interior pulsar magnetic field, and should be explored further with the addition of angular momentum conservation and other rotational effects.

At this point, further investigation into the idea of superfluidity is necessary. We made a first attempt at constraining the effects on braking index due to superfluidity, but this is insufficient in exploring the full consequences of superfluidity on spin evolution. We have tested a large scale effect of total core superfluidity, but this is a more 'static' description. We need to model the onset of superfluidity as a function of time in order to see a time rate effect on the braking index. The onset of superfluidity may lead to a dynamic differential rotation which may account for observed braking index values (Ho and Andersson, 2012), but this has not been fully realized as of yet. We would also like to investigate the effects of superfluidity on the magnetic field. Magnetic field expulsion and its consequential increase in surface magnetic field strength B, as they relate to the braking index should be considered.

Another, very important area of study is the EoS itself. It is hypothesized that at the extreme conditions of density in neutron star cores, there could exist a possible phase transition from hadronic matter to deconfined quark matter. This would represent a strong, first order phase transition in the EoS, which has the effect of softening the EoS significantly. The new state would require the star to have a further decrease in radius, a subsequent increase in density, and possibly become self-bound. All of which will lead to a temporary spin-up of the star, and subsequently, a likely significant effect on the dynamics of the braking index.

Bibliography

Agrawal, B. K., Shlom, S., and Au, V. K. (2005). *Phys. Rev. C*, 72:014310. 31

Alford, M. and Schwenzer, K. (2014). *ApJ*, 781:26. 9, 14, 24

Antoniadis, J. et al. (2013). *Science*, 340:448. 32

Arnett, W. D. and Bowers, R. L. (1977). A microscopic interpretation of neutron star structure. *Astrophys. J. Suppl.*, 33:415. 1

Baym, G. (1978). *Neutron Stars and the Physics of Matter at High Density*, volume 2 of *Nuclear Physics with Heavy Ions and Mesons*. ed. by Balian R. and Rho M. and Ripka G., North-Holland, Amsterdam. 1

Baym, G., Bethe, H., and Pethick, C. (1971a). *Nucl. Phys. A*, 175:299. 32

Baym, G., Pethick, C., and Sutherland, P. (1971b). *ApJ*, 170:299. 32

Blanford, R. D. and Romani, R. W. (1988). *MNRAS*, 234:570. 9, 10, 23, 24, 60, 80

Boyd, P. T., van Citters, G. W., Dolan, J. F., et al. (1995). *ApJ*, 448:365. 7

Carraminana, A. and Alvarez, C. (1996). *ASP Conference Series*, 105. 9, 24

Carraminana, A. and Alvarez, C. (2004). *Astron. Astrophys.*, 414:651. 9, 18, 19, 24, 81

Coburn, W. et al. (2003). *ApJ*, 580:394. 64

Contopoulos, I. and Spitkovsky, A. (2006). *ApJ*, 3642. 9, 18, 24, 60

Cook, G. B., Shapiro, S. L., and Teukolsky, S. A. (1992). *ApJ*, 398:203. 29

Demorest, P. B., Pennucci, T., Ransom, S. M., Roberts, M. S. E., and Hessels, J. W. T. (2010). *Nature*, 467:1081. 32

Dutra, M., Lourenco, O., Sa Martins, J. S., Delfino, A., Stone, J. R., and Stevenson, P. D. (2012). *Phys. Rev. C*, 85:035201. 31

ESA (2012). Welcome to the xmm-newton science operations centre. European Space Agency, http://xmm.esac.esa.int/ , accessed July 2012. 4

Espinoza, C. M., Lyne, A. G., Kramer, M., Manchester, R. N., and Kaspi, V. M. (2011). *ApJ*, 741:L13. ix, 7, 11

Eto, M., Hashimoto, K., and Hatsuda, T. (2013). *Phys. Rev. D*, 88:081701(R). 66

Fujisawa, K. and Kisaka, S. (2014). *MNRAS*, 445:2777. 64

G., L. A., Pritchard, R. S., Smith, F. G., and Camilo, F. (1996). *Nature*, 381:49. 7

Glendenning, N. K. (1985). Neutron stars are giant hypernuclei? *Astrophysical Journal*, 293:470. 1

Glendenning, N. K. (2000). *Compact Stars*. 2nd edition: Springer, New York. 12, 24, 25, 26

Glendenning, N. K., Pei, S., and Weber, F. (1997). *Phys. Rev. Lett.*, 79:1603. 26

Glenndenning, N. K. (2000). *Compact Stars, Nuclear Physics, Particle Physics, and General Relativity*, volume 2. Springer-Verlag, New York. 1

Gold, T. (1968). *Nature*, 218:731. 7, 14

Gold, T. (1969). *Nature*, 221:25. 7, 14

Goldreich, P. and Julian, W. H. (1969). *ApJ*, 157:869. 8

Goldwire, H. C. and Michel, F. C. (1969). *ApJ*, 156:L111. 6, 8, 14

Gourgouliatos, K. N. and Cumming, A. (2014). *arXiv:1406.3640*. 10, 24, 60

GSI (2012). Fair, facility for antiproton and ion research. GSI, http://www.gsi.de/en/start/fair/forschung-an-fair/kernmateriephysik.htm, accessed July 2012. xi, 3

Guichon, P. A. M., Matevosyan, H. H., Sandulescu, N., and Thomas, A. . (2006). *Nucl. Phys. A*, 772:1. 32

Haensel, P. and Bonazzola, S. (1996). *Astron. Astrophys.*, 314:1017. 64

Hamil, O. (2014). In Proceedings of Compact Stars in the QCD Phase Diagram IV (CSQCDIV), Prerow, Germany. 13

Hamil, O., Stone, J., Urbanec, M., and Urbancova, G. (2015). *Phys. Rev. D*, 91:063007. 21, 57, 64

Hamil, O. and Stone, J. R. (2015). *PRD (submitted)*. 58

Harding, A. K., Contopoulos, I., and Kazanas, D. (1999). *ApJ*, 525:L125. 9, 10, 14, 23, 24

Harding, A. K. and Lai, D. (2006). *Rep. Prog. Phys*, 69:2631. 64

Harrison, B. K. and Wheeler, J. A. (1965). cited in B. K. Harrison et al., Gravitation theory and gravitational collapse, Univ. of Chicago Press, Chicago. 32

Hartle, J. B. and Thorne, K. S. (1968). *ApJS*, 153:807. 29

Hartle, J. B. and Thorne, K. S. (1973). *Astrophysics and Space Science*, 24:385. 29

Hashimoto, K. (2015). *Phys. Rev. D*, 91:085013. 66, 77, 80

Ho, W. C. G. and Andersson, N. (2012). *Nature Physics*, 8:787. 11, 24, 38, 82

Hooker, J., Newton, W. G., and Li, B. A. (2013). *arXiv:1308.0031*. 38

Johnston, S. and Galloway, D. (1999). *MNRAS*, 306:L50. 11, 24

Kaspi, V. M., Mancheste, R. N., Siegman, B., Johnston, S., and Lyne, A. G. (1994). *ApJ*, 422:L83. 6, 9, 23

Komatsu, H., Eriguchi, Y., and Hachisu, I. (1989). *MNRAS*, 237:355. 29

Kramer, M., Lyne, A. G., O'Brie, J. T., Jordan, C. A., and Lorimer, D. R. (2006). *Science*, 312:549. 10, 23

Lattimer, J. M. and Prakash, M. (2004). The ultimate density of observable cold matter. *Physical Review Letters*, 94:1–4. 1

Liu, X.-W., Xu, R.-X., Guo-Jun, Q., Han, J.-L., and Tong, H. (2014). *Res. Astron. Astrophys.*, 14:85. 9, 11

Livingstone, M. A., Kaspi, V. M., Gavriil, F. P., et al. (2007). *Astron. Astroph.*, 308:317. 7

Livingstone, M. A., Ng, C. Y., Kasp, V. M., Gavriil, F. P., and Gotthelf, E. V. (2011). *ApJ*, 730:66. 7, 10, 18, 23

Lyne, A., Graham-Smith, F., Weltevrede, P., Jordan, C., Stappers, B., Bassa, C., and Kramer, M. (2013). *Science*, 342:598. 12, 24, 28, 55, 60, 61

Lyne, A., Hobbs, G., Kramer, M., Stairs, I., and Stappers, B. (2010). *Science*, 329:408. 10, 23

Lyne, A. G. (2004). Young neutron stars and their environments, ed. f. camilo and b. m. gaensler (san francisco, ca: Asp. *in IAU Symp.*, 218:257. 10, 23

Lyne, A. G., Jordan, A. G., Graham-Smith, F., Espinoza, C. M., Stappers, B. W., and Weltevrede, P. (2015). 45 years of rotation of the crab pulsar. *MNRAS*, 446:857. ix, 7, 14, 17, 23, 24, 25, 55, 58, 60, 61, 73, 77, 80

Lyne, A. G., Pritchard, R. S., and Smith, F. G. (1988). *MNRAS*, 233:667. 6, 9, 23

Lyne, A. G., Pritchard, R. S., and Smith, F. G. (1993). *MNRAS*, 265:1003. 7

Magalhaes, N. S., Miranda, T. A., and Frajuca, C. (2012). *ApJ*, 755:54:4pp. ix, 7, 12, 23, 24

Melatos, A. (1997). *MNRAS*, 288:1049. 10, 23, 60

Michel, F. C. (1969). *ApJ*, 157:1183. 7, 9, 14, 24

MPI (2012). The rosat mission. Max-Planck-Institut fr extraterrestrische Physik, http://www.mpe.mpg.de/xray/wave/rosat/index.php?lang=en, accessed July 2012. 4

Negele, J. W. and Vautherin, D. (1973). *Nucl. Phys. A*, 207:298. 32

Negreiros, R. (2012). *Numerical Study of the Properties of Compact Stars*. PhD thesis, Clairemont Graduate University, San Diego State University. 29, 79

Ostriker, J. P. and Gunn, J. E. (1969). *ApJ*, 157:1395. 7, 9, 14, 24

Ozel, F., Baym, G., and Guver, T. (2010). Astrophysical measurement of the equation of state of neutron star matter. *Physical Review D*, 82:10. 1

Pacini, F. (1967). *Nature*, 216:567. 7, 14

Pacini, F. (1968). *Nature*, 219:145. 7, 14, 25

Page, D., Lattimer, J. M., Prakash, M., and Steiner, A. W. (2014). *to be published in "Novel Superfluids", Eds. K. H. Bennemann and J. B. Ketterson*, volume 1. Oxford University Press. 11, 24, 38

Potekhin, A. Y. (2014). *Physics-Uspekhi*, 57:735. 64

Reisenegger, A. (2003). *Proceedings of the International Workshop on Strong Magnetic Fields and Neutron Stars*, page 31. 8, 64

Roy, J., Gupta, Y., and Lewandowski, W. (2012). *MNRAS*, 424:2213. 7

Sedrakian, A. and Cordes, J. M. (1998). *ApJ*, 502:378. 23, 38

Spruit, H. C. (2008). *AIP Conference Proceedings*, 983:391. 64

Steiner, A. W., Prakash, M., Lattimer, J. M., and Ellis, P. J. (2005). *Phys. Rep*, 411:325. 31

Stergioulas, N. and J. L. Friedman, J. L. (1995). *ApJ*, 444:306. 29

Stone, J. R., Guichon, P. A. M., Matevosyan, H. H., and Thomas, A. W. (2007). *Nucl. Phys. A*, 792:341. 32

Thompson, C. and Duncan, R. C. (1993). *ApJ*, 408:194. 64

Waltevrede, P., Johnson, S., and Espinoza, C. M. (2011). *MNRAS*, 411:1917. 7

Weber, F. (1999). *Pulsars as Astrophysical Laboratories for Nuclear and Particle Physics*, volume 1 of *High Energy Physics, Cosmology and Gravitation*. IOP Publishing, Bristol, Great Britain. 1, 29, 79

Weber, F. (2013). personal communication. xi, 2, 29, 79

Weber, F. and Weigel, M. K. (1989). *Nucl. Phys. A*, 505:779. 32

Zhang, S. N. and Xiee, Y. (2012). *ApJ*, 761:102. 9, 24, 60

Vita

Oliver Quinn Hamil grew up in the small town of San Luis Obispo, which is located on the central coast of California. He attended San Diego State University where he attained Bachelor of Science (2007), and a Master of Science (2012) degrees in physics. For both his Bachelor's and Master's degrees, his focus of study was on the properties of ultra-dense matter in neutron stars, and he wrote theses for both degrees under the advisment of Professor Fridolin Weber. After SDSU, Oliver attended the University of Tennessee to pursue his Ph.D. degree studying the spin evolution of neutron stars under the supervision of Professor Jirina R. Stone.